Fermi National Accelerator Laboratory

MPI-PAE/PTh 74/86
FERMILAB-PUB-86/163-T
December 1986

Testing the Standard Model versus a Composite Structure of Weak Interactions in High Precision Experiments at LEP and SLC

U. BAUR*

Fermi National Accelerator Lab.
P.O.Box 500, Batavia, IL 60510 (USA)

M. LINDNER

Max-Planck-Institut für Physik und Astrophysik
- Werner-Heisenberg-Institut für Physik -
P.O.Box 40 12 12, Munich (Fed. Rep. Germany)

K.H. SCHWARZER

Sektion Physik, University of Munich
Theresienstrasse 37, Munich (Fed. Rep. Germany)

ABSTRACT

Models with a composite structure of the weak interactions usually contain an isoscalar weak vector boson Y or Y_L which is coupled to the weak hypercharge current, or its lefthanded part. We study the impact of Y and Y_L on the Z-boson parameters and other measurables at future high energy e^+e^- colliders and discuss the corresponding standard model predictions. An analysis of the forward-backward and left-right asymmetry for the general case of two massive vector bosons with arbitrary vector and axial vector coupling constants is undertaken which may be applied to any other model containing additional weak vector bosons. If experiments at LEPI/SLC and LEPII agree with the standard model predictions within the possible experimental accuracies, $Y(Y_L)$-bosons with a mass of up to $1\ TeV$ $(0.9\ TeV)$ could be excluded.

---

* Max-Kade-Fellow

Operated by Universities Research Association Inc. under contract with the United States Department of Energy

1. Introduction

The standard Glashow-Weinberg-Salam (GSW) model [1] of electroweak interactions based on the gauge group $SU(2)_L$ x $U(1)_Y$ has achieved important successes in describing neutral and charged current processes and in correctly predicting [2] the mass of the W- and Z-bosons. However, essential ingredients of a renormalizable spontaneously broken gauge theory such as the standard model have not been confronted with experiment yet. In particular, the Yang-Mills structure of the self-couplings of the intermediate vector bosons and the Higgs-mechanism have not been tested. Moreover, experiments have not been accurate enough so far to probe the standard model much beyond tree level.

It is therefore still conceivable that the intermediate vector bosons are composite objects rather than the elementary gauge bosons of a spontaneously broken $SU(2)_L$ x $U(1)_Y$ gauge theory. Composite W- and Z-bosons occur in preon models of quarks and leptons [3] where the substructure scale Λ_H is related to the Fermi scale of the weak interactions, $\Lambda_H \sim G_F^{-1/2} \approx 300\ GeV$. If the preon Lagrangian is invariant under global $SU(2)_{WI}$ weak isospin transformations and vector dominance is invoked [4] such models yield the standard predictions for the neutral current structure and for the masses of W- and Z-bosons. On the other hand a spectrum of additional heavy vector bosons would constitute a main and direct experimental signature for such a richer short distance structure. The exact nature of this spectrum remains model dependant but some general features are nevertheless evident. Independently of the underlying preon model one always expects excited W's and Z's [5]. Furthermore, if the constituents of the intermediate vector bosons are colored objects, color octet partners of W and Z should appear [6] . Finally, many models predict additional isoscalar weak vector bosons with masses in the few hundred GeV range (see e.g. refs. [7], [8] and [9]).

While a direct exploration of such particles must, most likely, await the construction of a multi-TeV hadron-hadron collider [10], virtual effects of the new particles may already show up at much lower energies. In this paper we would like to discuss the effects of isoscalar weak vector bosons at LEPI/SLC and LEPII, and try to assess what the capabilities of these colliders are to set new limits on the parameters characterizing these particles. As a result, we shall conclude that,

provided that LEPII will be built, isoscalar weak vector bosons with a mass of up to 1 TeV can be excluded, or that necessarily deviations from the standard model have to show up.

Isoscalar weak vector bosons manifest themselves in high energy e^+e^- collisions in two different ways:

i) The physical Z-boson feels the mixing in of the new vector bosons. As a result, the exact values of the mass and the couplings of the Z will differ from the standard model predictions.

ii) Due to the exchange of an additional vector boson, the $e^+e^- \rightarrow \mu^+\mu^-$ cross-section and, even more importantly, the electroweak asymmetries may be significantly changed.

In our paper we shall discuss in depth both issues. In particular, we shall present an analysis of the electroweak asymmetries for the most general case of two massive vector bosons with completely arbitrary vector and axial-vector coupling constants. This analysis can be directly applied to models with composite isoscalar weak vector bosons, as well as to other models with new massive vector bosons like GUT's [11] , left-right symmetric [12] or superstring inspired [13] models. Our paper will, therefore, be also useful for studying asymmetries in such models. Given certain experimental accuracies for quantities measured at LEPI/SLC and LEPII, we shall then estimate limits on the parameters characterizing isoscalar weak vector bosons which one should be able to obtain, provided that no deviations from the standard model are observed. This will show us which quantity is most sensitive to the presence of isoscalar weak vector bosons, how useful polarization of the incident electron beam or the higher energy of LEPII are, and how accurately the standard model can be tested at future e^+e^- colliders.

Two possible scenarios for isoscalar weak vector bosons will be considered. In scenario A we investigate an isoscalar vector boson Y which couples to the weak hypercharge current. In scenario B, on the other hand, the isoscalar Y_L couples only to the lefthanded part of the weak hypercharge current. The first scenario corresponds to the situation where the preon Lagrangian has a global symmetry $G \supseteq SU(2)_{WI} \times U(1)_Y$, whereas scenario B may be realized if the compositeness scale of the righthanded sector is much larger than the one of the lefthanded sector,

or if righthanded quarks and leptons are elementary. Typical models of this type are the ones analyzed in refs. [7] and [9]. Here, only the lefthanded quarks and leptons are composite states. The Y_L-boson belongs to a 15-plet or a 143-plet of isoscalar vector bosons associated with a global $SU(4)$ or $SU(12)$ symmetry acting on the lefthanded fermions.

Our paper is organized as follows:

In Section 2 we consider the measurable quantities relevant for our purposes and give an overview over the corresponding standard model predictions. In Section 3 we discuss the influence of the $Y(Y_L)$ on the Z-mass and couplings and how this is reflected by measurable quantities at LEP and SLC. Section 4 is devoted to a careful analysis of the electroweak asymmetries. In the first part we shall present our general discussion of the asymmetries for two massive vector bosons which in the second part will be applied to the Y and Y_L. In Section 5, finally, we estimate those limits on the parameters characterizing the Y and Y_L which one should be able to derive from LEPI/SLC and LEPII experiments if no deviations from the standard model were to be observed. Section 6 contains our conclusions.

2. Measurables and their Standard Model Predictions

In this Section we would like to discuss the measurable quantities which we will employ in our subsequent analysis, and review the standard model predictions for them. We shall consider five quantities which are sensitive to the presence of additional heavy vector bosons: the masses of W and Z, m_W and M_Z, the leptonic width of the Z-boson and the electroweak asymmetries A_{FB} and A_{LR}.

2.1. THE Z-MASS M_Z

The most precise and most important quantity to be measured at LEPI and SLC is the Z-mass M_Z which will set the scale for high-precision tests of the electroweak theory. The errors on M_Z will be dominated by the uncertainty in determining the absolute energy scale E. If E can be measured with an accuracy of $\delta E/E = \pm 3 \cdot 10^{-4}$, M_Z can be obtained with an error of $\delta M_Z = 28\ MeV$ [14].

In the standard model M_Z is given by [15]

$$M_Z^2 = \frac{\mu^2}{\hat{s}^2 \hat{c}^2} \tag{2.1}$$

where $\hat{s}^2 = sin^2\theta_W$, θ_W is the Weinberg-angle, $\hat{c}^2 = 1 - \hat{s}^2$ and

$$\mu^2 = \frac{\mu_0^2}{1 - \Delta r} \tag{2.2}$$

with

$$\mu_0^2 = \frac{\pi\alpha(0)}{\sqrt{2}\, G_F} = (37.281\ GeV)^2\ . \tag{2.3}$$

Here, G_F denotes the Fermi-constant, $G_F = 1.166 \cdot 10^{-5} GeV^{-2}$, and $\alpha(0) \approx (137.04)^{-1}$ is the electromagnetic coupling constant. The quantity Δr in Eq. (2.2) represents the radiative corrections to M_Z at zero momentum transfer and depends on the t-quark mass m_t and the Higgs-boson mass m_H. For m_t smaller than the W-mass m_W, and m_H in the range from 10 GeV to 1 TeV one finds $\Delta r \approx 0.06...0.08$ [16]. The effects of radiative corrections can to a very good approximation be represented by writing

$$\mu^2 \simeq \mu_0^2\ \frac{\alpha(M_Z)}{\alpha(0)} \tag{2.4}$$

where $\alpha(M_Z)$ is the running electromagnetic coupling constant at the scale $m = M_Z$ [14]. Since Eq. (2.4) includes only QED contributions it ceases to be valid for heavy top quark masses (i.e. m_{top} in excess of $2m_W$).

2.2. THE W-MASS m_W

Since the Z-mass by itself alone does not say anything about the validity of the standard model and therefore will be used as a reference scale in experiments at LEPI/SLC, small deviations from the standard model in M_Z due to the presence of an additional neutral heavy vector boson will reveal themselves only if also the W-mass m_W is measured with an accuracy comparable to the one of the Z-mass measurement. This can be done directly at LEPII using the reaction $e^+e^- \rightarrow W^+W^-$ [17]. The resulting error in m_W is expected to be of the order of 100 MeV. However, a similar precision in the determination of the W-mass may also be possible by combining the results of LEPI/SLC and the improved CERN $p\bar{p}$ collider (ACOL) [14]. There, the ratio

$$\Delta = \frac{m_W}{M_Z} \tag{2.5}$$

will eventually provide a more precise test of the electroweak theory than the separate measurements of W- and Z-masses since it is free from the systematic error on the energy scale. With a realistic improvement of the detectors, such as that planned by UA1, one can presumably aim at a precision of [14]

$$\delta(\frac{m_W}{M_Z}) = \pm 2 \cdot 10^{-3} \ . \tag{2.6}$$

Combining this with the precision measurement of M_Z at LEPI/SLC yields an error in m_W of the order of 200 MeV. In the standard model, Δ coincides with $cos\theta_W$ and is only a function of M_Z. This can be easily seen by solving Eq.(2.1) for $\hat{s}^2$,

$$\hat{s}^2 = \frac{1}{2} - \left[\frac{1}{4} - \frac{\mu^2}{M_Z^2}\right]^{1/2} \tag{2.7}$$

which then yields

$$\Delta = \left\{\frac{1}{2} + \left[\frac{1}{4} - \frac{\mu^2}{M_Z^2}\right]^{1/2}\right\}^{1/2} \ . \tag{2.8}$$

2.3. THE LEPTONIC WIDTH OF THE Z-BOSON

While the masses of the intermediate vector bosons are directly accessable at LEPI/II and SLC, information on the Z- couplings can only be gained indirectly from a measurement of either the total Z-width Γ_Z or the leptonic width $\Gamma(Z \to \ell^+\ell^-)$; $\ell = e, \mu, \tau$. Γ_Z can be directly obtained from the line shape of the Z-peak with an error expected to be of the order of $\delta\Gamma_Z/\Gamma_Z \approx 2\%$ [14]. $\Gamma(Z \to \ell^+\ell^-)$, on the other hand, can be determined using the luminosity monitor [14]

$$I = \int \sigma(W)_{e^+e^- \to \ell^+\ell^-} dW = \frac{6\pi^2}{M_Z^2} \ \frac{\Gamma^2(Z \to \ell^+\ell^-)}{\Gamma_Z} \ . \tag{2.9}$$

If I can be measured with $\delta I/I \approx 3\%$, the leptonic Z-width can as well be obtained with an error of about 2 %.

From the point of view of testing the Z-couplings $\Gamma(Z \to \ell^+\ell^-)$ has to be preferred over Γ_Z. The reason for this is twofold. First of all, $\Gamma(Z \to \ell^+\ell^-)$ is a theoretically "clean" quantity which, in the standard model, can be accurately predicted once M_Z is known. Including electroweak radiative corrections one finds (neglecting the lepton masses)

$$\Gamma(Z \to \ell^+\ell^-) = \frac{G_F}{12\sqrt{2}\,\pi} M_Z^3 \ (1 - 4\hat{s}^2 + 8\hat{s}^4) \ (1 + \delta_\ell) \tag{2.10}$$

with $\hat{s}^2$ from Eq.(2.7). The quantity δ_ℓ represents the electroweak radiative correction and turns out to be very small if the radiatively corrected formula (2.7) is used for $\hat{s}^2$ [14]:

$$\delta_\ell \leq 0.1\% \; . \tag{2.11}$$

The total Z-width, on the other hand, is affected by strong interaction corrections and the uncertainty in the QCD coupling constant α_s introduces a theoretical error in Γ_Z of the order of 1 %. The second reason for preferring $\Gamma(Z \to \ell^+\ell^-)$ is that Γ_Z strongly depends on parameters such as m_t or the number of massless neutrino species which are presently completely unknown. In our subsequent analysis the total Z-width will, therefore, not be discussed further.

2.4. THE FORWARD-BACKWARD ASYMMETRY A_{FB}

Another observable at e^+e^- colliders which is particularily sensitive to additional heavy vector bosons and to the Lorentz-structure of their couplings is the integrated forward-backward asymmetry, defined by

$$A_{FB} = \frac{F - B}{F + B} \tag{2.12}$$

with

$$F \pm B = \left[\int_0^x \pm \int_{-x}^0 \right] dz \; \frac{d\sigma(e^+e^- \to f\bar{f})}{dz} \; ; \tag{2.13}$$

z is the cosine of the angle between the fermion f and the beam direction and x the detector acceptance ($x \leq 1$). The most precise determination of A_{FB} can be performed on the Z-peak and if the final state fermions consist of muons. For an integrated luminosity of $\int \mathcal{L} dt = 100 \; pb^{-1}$ the experimental error is estimated to be [18]

$$\delta A_{FB}^{e^+e^- \to \mu^+\mu^-}(M_Z) \approx 3 \cdot 10^{-3} \; . \tag{2.14}$$

For comparison, at the highest projected LEPII energy of $\sqrt{s} = 190 \; GeV$ and with an integrated luminosity of 500 pb^{-1} the experimental error is expected to be about a factor ten larger than at resonance [18], i.e.

$$\delta A_{FB}^{e^+e^- \to \mu^+\mu^-}(190 \; GeV) \approx 0.03 \; . \tag{2.15}$$

The values for the integrated luminosities used above are typical estimates for a 100 day running period at LEPI/II with unpolarized beams. If the electron beam

at LEPI/II could achieve a 50 % longitudinal polarization, as it will be possible at the SLC, the expected luminosity would be about a factor 2.5 smaller and the errors in A_{FB} would increase by about a factor 1.6 [18].

In the standard model, the tree-level expression for A_{FB} is given by

$$A_{FB}^{e^+e^-\to\mu^+\mu^-} = \frac{x}{1+\frac{x^2}{3}} \ \frac{N}{D} \tag{2.16}$$

with

$$N = \frac{e^2}{4s}\, g_Z^2\, \frac{s-M_Z^2}{\rho(s)}\, (1+P_e v_e) + \frac{g_Z^4}{64}\, \frac{v_e}{\rho(s)}\, [2v_e + P_e(1+v_e^2)]\ , \tag{2.17}$$

$$D = 2\,\frac{e^4}{s^2} + \frac{e^2}{4s}\, g_Z^2\, \frac{s-M_Z^2}{\rho(s)}\, v_e\ (P_e+v_e) + \frac{g_Z^4}{128}\, \frac{1+v_e^2}{\rho(s)}\ (1+v_e^2+2P_e v_e) \tag{2.18}$$

where

$$\rho(s) = (s-M_Z^2)^2 + M_Z^2\Gamma_Z^2\ ; \tag{2.19}$$

s is the center of mass energy squared, $g_Z = g_W/cos\theta_W$, $g_W^2 = 4\sqrt{2}G_F m_W^2$, P_e is the degree of the longitudinal polarization of the e^--beam and

$$v_e = 1 - 4sin^2\theta_W \tag{2.20}$$

is the Z vector coupling constant for charged leptons. The expression of A_{FB} for an unpolarized e^--beam can be obtained by setting $P_e = 0$ in Eqs. (2.16) to (2.18). Note that all terms containing P_e in Eqs. (2.17) and (2.18) are proportional to v_e, which is small because $sin^2\theta_W$ is close to 1/4. Longitudinal polarization will, therefore, only slightly affect the shape of A_{FB} in the standard model.

The expression for A_{FB} considerably simplifies on top of the Z-peak ($s = M_Z^2$). In the narrow width approximation ($\Gamma_Z \ll M_Z$) we find

$$A_{FB}^{e^+e^-\to\mu^+\mu^-} = 2\ \frac{x}{1+\frac{x^2}{3}}\ \frac{v_e}{1+v_e^2}\ \frac{2v_e + P_e(1+v_e^2)}{1+v_e^2+2P_e v_e}\ . \tag{2.21}$$

In Fig. 1 we show the forward-backward asymmetry versus $\sqrt{s}$ for $P_e = 0$ and $x = 1$. As one can see, $A_{FB}^{e^+e^-\to\mu^+\mu^-}$ varies strongly in the neighbourhood of the Z-resonance with a zero at ($P_e = 0$)

$$s = M_Z^2\ \Big[1 + \frac{v_e^2}{8sin^2\theta_W cos^2\theta_W}\Big]^{-1} \tag{2.22}$$

and a minimum (maximum) at (for $\Gamma_Z \ll M_Z$, $P_e = 0$)

$$\frac{s}{s - M_Z^2} = \frac{16\ \sin^2\theta_W \cos^2\theta_W}{(1+v_e^2)^2}\left[2v_e^2 \mp (4v_e^4 + (1+v_e^2)^2)^{1/2}\right] . \qquad (2.23)$$

For $M_Z = 92\ GeV$ the numerical values are $\sqrt{s}(A_{FB} = 0) \approx 91.8\ GeV$, $\sqrt{s}_{min} \approx 78.9\ GeV$ and $\sqrt{s}_{max} \approx 114.3\ GeV$.

Electroweak radiative corrections are known to influence A_{FB} significantly. In general the corrected asymmetry can be written down as a sum of three terms:

$$A_{FB} = A_{FB}^{Born} + \delta A_{FB}^{QED} + \delta A_{FB}^{weak} . \qquad (2.24)$$

Some one-loop corrections can already be included by using the radiatively corrected value of $sin^2\theta_W$. δA_{FB}^{QED} represents the real and virtual photon emission and the one-loop photon vacuum polarization diagrams which contribute to the running α which is already contained in (2.4). Finally, δA_{FB}^{weak} are the purely weak corrections to A_{FB} which depend on the unknown quantities m_t and m_H. At resonance, δA_{FB}^{weak} is a sizeable fraction of A_{FB}^{Born} and rather sensitve to m_t and m_H. For $30\ GeV \leq m_t \leq 180\ GeV$, $10\ GeV \leq m_H \leq 1\ TeV$ and $90\ GeV \leq M_Z \leq 98\ GeV$, δA_{FB}^{weak} can vary by as much as ± 0.01 [19].

2.5. THE LEFT-RIGHT ASYMMETRY A_{LR}

The final quantity we want to discuss is the left-right asymmetry A_{LR}. It requires a longitudinal polarization for the e^--beam and is given by

$$A_{LR} = \frac{\sigma_L - \sigma_R}{\sigma_L + \sigma_R} \qquad (2.25)$$

where $\sigma_{L,R}$ are the cross-sections for $e^-_{L,R} + e^+ \rightarrow X$, and X can be any channel. The most precise determination of A_{LR} will be possible on top of the Z-resonance: for an integrated luminosity of 40 pb^{-1} with a 50 % longitudinally polarized e^--beam the error is estimated to be [18]

$$\delta A_{LR}(M_Z) \approx 1.5 \cdot 10^{-3} \qquad (2.26)$$

whereas for e.g. $\sqrt{s} = 190\ GeV$ and $\int \mathcal{L} dt = 200\ pb^{-1}$ [18]

$$\delta A_{LR}(190\ GeV) \approx 0.02 . \qquad (2.27)$$

In the standard model, the tree-level expression for A_{LR} reads

$$A_{LR} = P_e \, \frac{N'}{D'} \tag{2.28}$$

with

$$N' = \frac{e^2}{2s} \mid e_f \mid \; g_Z^2 \, v_f \, \frac{s - M_Z^2}{\rho(s)} + \frac{g_Z^4}{32} \, v_e \, \frac{1 + v_f^2}{\rho(s)} \; , \tag{2.29}$$

$$D' = 4 \, \frac{e^4}{s^2} \, e_f^2 + \frac{e^2}{2s} \mid e_f \mid \; g_Z^2 \, v_e \, v_f \, \frac{s - M_Z^2}{\rho(s)} + \frac{g_Z^4}{64} \, (1 + v_f^2) \, \frac{1 + v_e^2}{\rho(s)} \tag{2.30}$$

and where e_f is the electric charge (in units of e) and

$$v_f = 1 - 4 \mid e_f \mid sin^2\theta_W \tag{2.31}$$

is the vector coupling constant of the final state fermion f which we supposed to be massless. The above expression for A_{LR} considerably simplifies on the Z-peak if the narrow width approximation is used. One finds

$$A_{LR}(M_Z) = 2P_e \, \frac{v_e}{1 + v_e^2} \; . \tag{2.32}$$

Note that $A_{LR}(M_Z)$ is *independent* from the vector coupling constants of the final state fermions and, therefore, the same for all fermions with masses much smaller than M_Z, except e and ν_e. In Section 4 we shall show that this is a unique feature of the standard model which is destroyed if a second massive vector boson is present. Comparing A_{LR} in different channels on top of the Z-resonance will, therefore, be another important test for the standard model at LEPI/SLC.

In Fig.1 we show A_{LR}/P_e versus $\sqrt{s}$ for the channel $e^+e^- \to \mu^+\mu^-$. Since $A_{LR}^{e^+e^- \to \mu^+\mu^-}$ is proportional to the vector coupling constant v_e, which itself is small, the left-right asymmetry does not vary very much. Similar to A_{FB},A_{LR} has one zero which is located at

$$s = M_Z^2 \left[1 + \frac{1 + v_e^2}{16 sin^2\theta_W cos^2\theta_W}\right]^{-1} \tag{2.33}$$

and one minimum (maximum) at ($\Gamma_Z \ll M_Z$)

$$\frac{s}{s - M_Z^2} = \frac{16 \sin^2\theta_W \cos^2\theta_W}{1 - v_e^4} \left[1 + v_e^2 \mp (2(1 + v_e^2))^{1/2}\right] \tag{2.34}$$

in the standard model. The numerical values for $M_Z = 92\ GeV$ are $\sqrt{s}(A_{LR} = 0) \approx 79\ GeV$, $\sqrt{s}_{min} \approx 67\ GeV$ and $\sqrt{s}_{max} \approx 100\ GeV$.

Finally, we briefly discuss electroweak radiative corrections to A_{LR}. Some of them can be included by using the radiatively corrected value of $sin^2\theta_W$. Similar to the case of the forward-backward asymmetry, the purely weak corrections turn out to be a sizeable fraction of the Born term on top of the Z-resonance and are sensitive to m_t and m_H. They can vary by as much as ± 0.02 for $30\ GeV \leq m_t \leq 180\ GeV$, $10\ GeV \leq m_H \leq 1\ TeV$ and $90\ GeV \leq M_Z \leq 98\ GeV$ [19].

3. Isoscalar Weak Vector Bosons and Z-Boson Parameters

We now turn to a more detailed discussion of the composite weak boson scenarios which we have briefly described in the introduction. In the first part of this Section we develop the effective Lagrangian formalism used to describe composite weak boson interactions and derive the Lagrangian for interactions of the Z-boson with quarks and leptons as well as the expression for the Z-mass in the presence of isoscalar weak vector bosons. In the second part we shall analyze how Y and Y_L affect the observable quantities m_W/M_Z and $\Gamma(Z \to \ell^+\ell^-)$.

3.1. Effective Lagrangian Formalism

To describe the interactions of fermions with the isotriplet of weak bosons, $\mathbf{W}$, and the isoscalar $Y(Y_L)$ we use an effective Lagrangian. The weak isospin $SU(2)_{WI}$ symmetry is supposed to be a global symmetry of the underlying preon model in the limit of a vanishing electromagnetic coupling constant $e = \sqrt{4\pi\alpha}$. The effective Lagrangian for the interaction of $\mathbf{W}$ and $Y(Y_L)$ with quarks and leptons in the limit $\alpha \to 0$ is given by

$$\mathcal{L} = g_W \mathrm{j}_{\mu L} \mathbf{W}_\mu + g_Y j_\mu^{Y_{(L)}} \tilde{Y}_{(L)\mu} \tag{3.1}$$

where $\mathbf{W}_\mu$ and $\tilde{Y}_{(L)\mu}$ describe the $\mathbf{W}$- and $Y(Y_L)$-field and

$$\mathrm{j}_{\mu L} = \sum_L \bar{L}\gamma_\mu \frac{\tau}{2} L\ ,$$

$$j_\mu^Y = j_\mu^{Y_L} + \sum_R \bar{R}\gamma_\mu y_R R\ , \tag{3.2}$$

$$j_\mu^{Y_L} \equiv j_{\mu L}^{Y} = \sum_L \bar{L}\gamma_\mu y_L L$$

are the weak isospin and hypercharge currents; $j_\mu^{Y_L}$ is the lefthanded part of j_μ^Y, $L(R)$ runs over all lefthanded (righthanded) fermion $SU(2)_{WI}$ doublets (singlets), τ are the Pauli-matrices and $y_L = Q - T_3$ and $y_R = Q$ are the respective hypercharge quantum numbers. Q and T_3, finally, denote the electric charge and the third component of the weak isospin, respectively.

For $\alpha \neq 0$, the result of Eq. (3.1) is modified by the mixing of $Y(Y_L)$ and W^3 with the photon [20] ($V_{\mu\nu} = \partial_\mu V_\nu - \partial_\nu V_\mu$; $V = W^3$, $\tilde{Y}_{(L)}$; $\tilde{F}_{\mu\nu} = \partial_\mu \tilde{A}_\nu - \partial_\nu \tilde{A}_\mu$)

$$\mathcal{L}_{mix} = -\frac{1}{4}\lambda_W(\tilde{F}_{\mu\nu}W^{3\mu\nu} + \tilde{F}^{\mu\nu}W^3_{\mu\nu}) - \frac{1}{4}\lambda_Y(\tilde{F}_{\mu\nu}\tilde{Y}^{\mu\nu}_{(L)} + \tilde{F}^{\mu\nu}\tilde{Y}_{(L)\mu\nu}) \qquad (3.3)$$

where $\tilde{A}_\mu$ denotes the photon field. This mixing and the saturation of the electromagnetic form factors by massive vector bosons (W^3- and $Y(Y_L)$-dominance [4]) relates the mixing strengths λ_W and λ_Y to the electric charge unit e via

$$g_W\lambda_W = g_Y\lambda_Y = e\ . \qquad (3.4)$$

The W^3- and $Y(Y_L)$-vector boson dominance thus implies a universal coupling of the fermions to the respective vector bosons, namely g_W and g_Y.

The physical content of the model can easily be obtained after removing the mixing term by the nonunitary transformation

$$\begin{pmatrix} \tilde{A}_\mu \\ W^3_\mu \\ \tilde{Y}_{(L)\mu} \end{pmatrix} = \begin{pmatrix} 1 & -\frac{1}{b_Z} & -\frac{1}{b_Y} \\ 0 & -\frac{\lambda_W}{b_Z}\frac{M_Z^2}{m_W^2 - M_Z^2} & -\frac{\lambda_W}{b_Y}\frac{M_Y^2}{m_W^2 - M_Y^2} \\ 0 & -\frac{\lambda_Y}{b_Z}\frac{M_Z^2}{m_Y^2 - M_Z^2} & -\frac{\lambda_Y}{b_Y}\frac{M_Y^2}{m_Y^2 - M_Y^2} \end{pmatrix} \begin{pmatrix} A_\mu \\ Z_\mu \\ Y_{(L)\mu} \end{pmatrix} \ . \qquad (3.5)$$

Here, A_μ, Z_μ and $Y_{(L)\mu}$ denote the physical photon, Z- and $Y(Y_L)$-fields,

$$b_i^2 = 1 - \lambda_W^2 - \lambda_Y^2 + \lambda_W^2\ \frac{m_W^4}{(m_W^2 - M_i^2)^2} + \lambda_Y^2\ \frac{m_Y^4}{(m_Y^2 - M_i^2)^2} \qquad (3.6)$$

with $i = Z, Y$ and M_Y is the physical $Y(Y_L)$-mass. The unobservable "bare" mass m_Y (before mixing with the photon) of the $Y(Y_L)$-boson and λ_W can be related to M_Y and G_F by [10]

$$m_Y^2 = M_Y^2\ (1 - \lambda_Y^2\ \frac{M_Y^2 - m_W^2}{(1 - \lambda_W^2)M_Y^2 - m_W^2})\ , \qquad (3.7)$$

$$\lambda_W^2 = \frac{e^2}{m_W^2}\frac{\sqrt{2}}{8}G_F^{-1} \ . \tag{3.8}$$

According to Eqs. (3.4) - (3.7), the effects of $Y(Y_L)$ are characterized by the two parameters λ_Y and M_Y. Since m_Y^2 has to be nonnegative, λ_Y^2 is bounded from above by [10]

$$\lambda_Y^2 \leq \lambda_{Y\,max}^2 = 1 - \lambda_W^2 \frac{M_Y^2}{M_Y^2 - m_W^2} < 1 - \lambda_W^2 \ . \tag{3.9}$$

Using the transformation Eq. (3.5) we can now determine the Z-mass and the effective Lagrangian for the interactions of the Z-boson with quarks and leptons. We find:

$$M_Z^2 = \frac{m_W^2}{1 - \lambda_W^2 - \lambda_Y^2}\ \frac{m_Y^2}{M_Y^2} \tag{3.10}$$

and

$$\mathcal{L}_{Zf\bar{f}} = \tilde{g}_Z\ [j_{\mu L}^3 + \delta j_\mu^{Y(L)} - s_W^2 j_\mu^{em}]\ Z_\mu \ , \tag{3.11}$$

where $j_{\mu L}^3$ denotes the third component of the weak isospin current, j_μ^{em} the electromagnetic current,

$$\tilde{g}_Z = \frac{e}{b_Z}\ \frac{M_Z^2}{M_Z^2 - m_W^2} \tag{3.12}$$

$$\delta = \frac{M_Z^2 - m_W^2}{M_Z^2 - m_Y^2} \tag{3.13}$$

and, finally,

$$s_W^2 = 1 - \frac{m_W^2}{M_Z^2} \ . \tag{3.14}$$

Note that s_W^2 formally agrees with $sin^2\theta_W$ which multiplies the j_μ^{em} term in the standard model.

Eqs. (3.10) - (3.14) show that in presence of $Y(Y_L)$ the Z-mass and couplings deviate from the standard model predictions. In addition to the weak isospin and the electromagnetic current, the Z-boson couples also to $j_\mu^Y\,(j_\mu^{Y_L})$ with relative strength δ which for $M_Y^2 \gg m_W^2$ can approximately be written as

$$\delta \approx -\frac{\lambda_W^2}{1 - \lambda_W^2 - \lambda_Y^2}\ \frac{m_W^2}{M_Y^2} \ . \tag{3.15}$$

If M_Y lies in the few hundred GeV range, as one should naively expect in a preon model with a scale $\Lambda_H \sim O(G_F^{-1/2})$, the absolute value of δ is of the order of a few percent.

For the subsequent discussion of the leptonic width of the Z-boson and the electroweak asymmetries, it is convenient to express $\mathcal{L}_{Zff}$ in terms of vector and axial vector coupling constants $V_Z^Y(V_Z^{Y_L})$ and $A_Z^Y(A_Z^{Y_L})$ respectively. One obtains

$$\mathcal{L}_{Zff} = Z_\mu \left[\sum_f \bar{f}\gamma_\mu \frac{1}{2}(V_Z^{Y_{(L)}} + A_Z^{Y_{(L)}}\gamma_5) f\right] \tag{3.16}$$

where in the Y-case

$$A_Z^Y = \frac{e}{b_Z}\,\frac{M_Z^2}{M_Z^2 - m_W^2}\,\frac{m_Y^2 - m_W^2}{M_Z^2 - m_Y^2}\,T_3 \tag{3.17}$$

$$V_Z^Y = 2\frac{e}{b_Z}\,\frac{m_Y^2}{M_Z^2 - m_Y^2}Q - A_Z^Y \tag{3.18}$$

and in the Y_L-case

$$A_Z^{Y_L} = -\frac{e}{b_Z}\,\frac{M_Z^2}{M_Z^2 - m_Y^2}Q + A_Z^Y \tag{3.19}$$

$$V_Z^{Y_L} = -\frac{e}{b_Z}(1 - \frac{m_Y^2}{M_Z^2 - m_Y^2})Q - A_Z^Y\ . \tag{3.20}$$

In Eqs. (3.17) - (3.20) we have used that $y_L = Q - T_3$ and $y_R = Q$.

In the limit of a vanishing $Y(Y_L)$-photon mixing strength λ_Y Eq. (3.10) reduces to the standard model expression for M_Z. This can be easily seen by observing that $m_Y^2 \to M_Y^2$ for $\lambda_Y^2 \to 0$ (see Eq. (3.7)) and using Eq. (3.8) for λ_W^2. In this limit also $\tilde{g}_Z$ and s_W^2 approach their standard model values $e/sin\theta_W cos\theta_W$ and $sin^2\theta_W$, respectively. However, since $g_Y\lambda_Y = e$ (see Eq. (3.4)) is a constant, δ does *not* go to zero for $\lambda_Y^2 \to 0$. For small values of λ_Y^2 we find

$$\delta \approx -\frac{\lambda_W^2 m_W^2}{(1-\lambda_W^2)M_Y^2 - m_W^2}(1 + \lambda_Y^2\frac{M_Y^2 - m_W^2}{(1-\lambda_W^2)M_Y^2 - m_W^2})\ . \tag{3.21}$$

δ vanishes only for $M_Y \to \infty$.

Eqs. (3.7) - (3.14) represent the tree-level results for the mass and the couplings of the Z-boson. Since we are interested in implications of $Y(Y_L)$ at LEPI/SLC and

LEPII energies, i.e. at a scale $\mu^2 \geq M_Z^2$, we should also take into account radiative corrections. However, the effective theory of composite weak vector bosons we are working with is nonrenormalizable and a full renormalization program, therefore, cannot be carried out. Nevertheless, the evolution of the leading log corrections can be done in the framework of the effective field theory approach [21] and this modifies e (there are no leading log corrections to G_F) in the same way as in the standard model, provided that the particle spectrum below m_W is the same. Vector dominance guarantees that the corrections to α are finite to all orders in perturbation theory [22]. Subsequently, we, therefore, shall use the radiatively improved value of e (i.e. $\alpha \approx 1/128$) in Eqs. (3.4), (3.8), (3.12) and (3.17) - (3.20).

3.2. Penomenological Implications

Using the expressions for the Z-mass (Eq. (3.10)) and the vector and axial vector coupling constants (Eq. (3.17) - (3.20)) it is now rather straightforward to study the implications of $Y(Y_L)$ on measurable quantities. Here, we would like to concentrate on two observables: the ratio m_W/M_Z, which, as we have discussed in Section 2, can hopefully be measured very accurately at ACOL, and the leptonic width of the Z-boson. The influence of $Y(Y_L)$ on electroweak asymmetries will be discussed in detail in Section 4.

In Fig. 2 we present plots for m_W/M_Z versus M_Z for various values of M_Y and λ_Y^2. Fig. 2a shows the variation of m_W/M_Z with λ_Y^2 for $M_Y = 500\ GeV$, whereas Fig. 2b illustrates how m_W/M_Z versus M_Z behaves as a function of M_Y for $\lambda_Y^2 = 0.2$. For values of M_Y and λ_Y^2 different from those chosen in Fig. 2a and 2b respectively, curves of a similar shape are obtained. For comparison, we have also included in Fig. 2 the standard model prediction for m_W/M_Z taking into account leading log corrections (see Eqs. (2.4) and (2.8)) which, as we have seen in Section 2, very accurately represent the complete $O(\alpha)$ corrections to m_W and M_Z.

Before we discuss Fig. 2 in more detail we would like to make a general remark about how one should compare standard model and composite weak boson model results. Since we can only include leading log corrections in the effective theory we are working with, composite weak boson model predictions should be compared with standard model calculations where also only leading log correc-

tions have been taken into account. A comparison with the results of a complete one-loop calculation would make sense only if one could carry out a full renormalization program for the effective theory of composite weak boson interactions. This is, however, not possible since the effective theory is nonrenormalizable and we, therefore, cannot do better than comparing composite W-boson model and standard model predictions both at the leading log level.

From Fig. 2 we observe that the Y- and Y_L-boson affect the ratio m_W/M_Z in the same way. Furthermore, we see that m_W/M_Z is always larger than in the standard model and increases (decreases) with increasing values of λ_Y^2 (M_Y). In the limit $\lambda_Y^2 \to 0$ (for fixed M_Y) and $M_Y \to \infty$ (for fixed λ_Y^2) we recover the standard model prediction for m_W/M_Z.

In Fig. 3 we display the leptonic Z-width (lepton masses are neglected)

$$\Gamma(Z \to \ell^+\ell^-) = \frac{M_Z}{48\pi}\,(V_Z^{Y_{(L)}^2} + A_Z^{Y_{(L)}^2})\,, \tag{3.22}$$

$\ell = e, \mu, \tau$, versus M_Z for various values of λ_Y^2 and M_Y, together with the standard model prediction in the leading log approximation which we obtain by setting $\delta_\ell = 0$ in Eq. (2.10) and employing Eqs. (2.4) and (2.7). Fig. 3a shows how $\Gamma(Z \to \ell^+\ell^-)$ changes with λ_Y^2 for $M_Y = 500\ GeV$ while Fig. 3b presents results for $\lambda_Y^2 = 0.2$ when M_Y is varied. For values of M_Y and λ_Y^2 different from those in Fig. 3a and 3b respectively, curves of a similar shape are obtained. As one can see, Y and Y_L influence the leptonic Z-width in a completely different way. While $\Gamma(Z \to \ell^+\ell^-)$ is in the Y-case larger than in the standard model, the contrary is true if the underlying preon model contains a Y_L-boson. For increasing M_Y (λ_Y^2) the deviation of the leptonic Z-width from its standard model value decreases (increases) and vanishes in the limit $M_Y \to \infty$. On the other hand, since δ remains finite for $\lambda_Y^2 \to 0$ (see Eq. (3.21)), $\Gamma(Z \to \ell^+\ell^-)$ may differ appreciably from the standard model result even for very small values of λ_Y^2. This is illustrated by the two $\lambda_Y^2 = 0.0$ curves in Fig. 3a.

From Fig. 2 and Fig. 3 we recognize that both, m_W/M_Z and $\Gamma(Z \to \ell^+\ell^-)$, may be significantly affected by the $Y(Y_L)$-boson. High precision measurements of M_Z, m_W/M_Z and the leptonic Z-width should, therefore, result in rather stringent bounds on the parameters M_Y and λ_Y^2, provided that no deviations from the

standard model are observed. We will return to these questions in detail in Section 5.

4. Electroweak Asymmetries

We will now consider the electroweak asymmetries in more detail. In the first part of this Section we shall present the tree-level expressions for A_{FB} and A_{LR} for the most general case of two massive vector bosons with completely arbitrary vector and axial vector coupling constants and discuss some of their properties. Special emphasis will be given to the location of the zeros of A_{FB} and A_{LR} since this will give us some hints how the shape of the electroweak asymmetries versus $\sqrt{s}$ in the two vector boson case might look like, and how big the deviations from the standard model predictions might be. In the second part of this Section we study A_{FB} and A_{LR} in the Y- and Y_L-case, thereby verifying the correctness of the results of the general analysis in the first part.

4.1. General Discussion

We start with some definitions. We assume that in addition to the photon two massive neutral vector bosons V_i and V_j, with masses M_i and M_j, contribute to the reaction $e^+e^- \to f\bar{f}$ in the s-channel. The $V_k f\bar{f}$, $k = i, j$, vector and axial vector coupling constants are denoted by v_{kf} and a_{kf}, respectively. Finally, $\Gamma_{i,j}$ is the total width of $V_{i,j}$.

Using the definitions (2.12), (2.13) and (2.25) it is now straightforward to calculate the tree-level expressions for $A_{FB}^{e^+e^-\to f\bar{f}}$ and $A_{LR}^{e^+e^-\to f\bar{f}}$, $f \neq e, \nu_e$. One obtains

$$A_{FB}^{e^+e^-\to f\bar{f}} =$$

$$\frac{x}{1+\frac{x^2}{3}} \frac{(1-P_e)\sum_{h_f,h_e} h_f h_e \mid F(h_f,h_e)\mid^2 + 2P_e \sum_{h_f} h_f \mid F(h_f,1)\mid^2}{(1-P_e)\sum_{h_f,h_e} \mid F(h_f,h_e)\mid^2 + 2P_e \sum_{h_f} \mid F(h_f,1)\mid^2} \tag{4.1}$$

and

$$A_{LR}^{e^+e^-\to f\bar{f}} = P_e \frac{\sum_{h_f,h_e} h_e \mid F(h_f,h_e)\mid^2}{\sum_{h_f,h_e} \mid F(h_f,h_e)\mid^2} \tag{4.2}$$

where

$$F(h_f,h_e) =$$

$$-\frac{e^2}{s}e_f+\frac{1}{4}\,\frac{(v_{if}-h_f a_{if})(v_{ie}-h_e a_{ie})}{s-M_i^2+iM_i\Gamma_i}+\frac{1}{4}\,\frac{(v_{jf}-h_f a_{jf})(v_{je}-h_e a_{je})}{s-M_j^2+iM_j\Gamma_j} \qquad (4.3)$$

and $h_{f,e}=\pm 1$ are the helicities of f and e, respectively.

While Eqs. (4.1) - (4.3) are in a form convenient for numerical evaluation, they offer little insight into the general properties of A_{FB} and A_{LR}. However, if V_i and V_j couple universally to charged leptons, some information on the electroweak asymmetries for the most important channel $e^+e^-\to\mu^+\mu^-$ may be gained by performing the sums in Eqs. (4.1) and (4.2). It turns out that

i) if one of the resonances couples in a purely righthanded way to charged leptons it has no influence on A_{FB} if the incident electron beam is fully lefthandedly polarized, i.e. if $P_e=1$.

ii) if both, V_i and V_j couple purely vector like, or if one vector boson couples vector like and the other one axial vector like to charged leptons, A_{FB} is *independent* of P_e and A_{LR} vanishes.

iii) $A_{LR}(M_Z)$ depends in general on the final state fermion vector and axial vector coupling constants, contrary to the one boson case (see Eq. (2.32)).

In general, useful information on the shape of A_{FB} and A_{LR} versus $\sqrt{s}$ can be obtained from the positions of the maxima, minima and zeros of the electroweak asymmetries. While we were not able to find analytical solutions for the minima and maxima, it is easy to see that requiring $A_{FB}=0$ and $A_{LR}=0$, respectively, leads in both cases to equations cubic in s. Therefore, there are *at most* three zeros (apart from a trivial one at $s=0$) in A_{FB} and A_{LR}.

In view of practical applications where one of the massive vector bosons has to be identified with the Z-boson, let us study in somewhat greater detail the zeros in the case of $e^+e^-\to\mu^+\mu^-$ where

a) V_i and V_j couple universally to charged leptons and where

b) we assume

$$\Gamma_i\ll M_i \text{ and } v_{ie}\approx 0 \qquad (4.4)$$

Under these simplifying assumptions we find for the zeros in $A_{FB}^{e^+e^-\to\mu^+\mu^-}$

$$s_1=M_i^2 \qquad (4.5)$$

$$s_{2,3} = M_j^2 + \frac{1}{2A}\left(-B \pm \sqrt{B^2 - 4AC}\right) \tag{4.6}$$

with

$$A = 2e^2(a_{ie}^2 + \gamma_{je}a_{je}^2) + \frac{1}{2}v_{je}^2a_{je}^2(\gamma_{je} + \delta_{je}) + \frac{1}{2}v_{je}^2a_{ie}^2\delta_{je}\ , \tag{4.7}$$

$$B = 2e^2a_{je}^2\gamma_{je}(M_j^2 - M_i^2) + \frac{1}{2}v_{je}^2a_{ie}^2\delta_{je}M_j^2 + \frac{1}{2}v_{je}^2a_{je}^2(\gamma_{je}+\delta_{je})(2M_j^2 - M_i^2)\ , \tag{4.8}$$

$$C = \frac{1}{2}v_{je}^2a_{je}^2M_j^2(M_j^2 - M_i^2)(\gamma_{je} + \delta_{je}) + 2e^2a_{ie}^2M_j^2\Gamma_j^2\ , \tag{4.9}$$

$$\gamma_{je} = 1 - P_e\,\frac{v_{je}}{a_{je}}\ , \tag{4.10}$$

$$\delta_{je} = 1 - P_e\,\frac{a_{je}}{v_{je}}\ , \tag{4.11}$$

and for the zeros in $A_{LR}^{e^+e^-\to\mu^+\mu^-}$ we derive

$$S_1 = M_i^2\ , \tag{4.12}$$

$$S_{2,3} = \frac{1}{2A}\left(-B \pm \sqrt{B^2 - 4AC}\right)\ , \tag{4.13}$$

with

$$A = 2e^2 + \frac{1}{2}\left(a_{ie}^2 + v_{je}^2 + a_{je}^2\right)\ , \tag{4.14}$$

$$B = -(2e^2 + \frac{1}{2}a_{ie}^2)M_j^2 - (2e^2 + \frac{1}{2}v_{je}^2 + \frac{1}{2}a_{je}^2)M_i^2\ , \tag{4.15}$$

$$C = 2e^2M_i^2M_j^2\ . \tag{4.16}$$

From Eqs. (4.5) - (4.16) a number of useful observations can be made:

1) Comparing Eq. (4.5) with Eq. (2.22) (for $v_e = 0$) shows that the first zero in $A_{FB}^{e^+e^-\to\mu^+\mu^-}$ is (almost) unaffected by the existence of a second massive vector boson if the first one couples (almost) purely axial vector like.

2) The second and third zeros, $s_{2,3}$ and $S_{2,3}$, exist if $B^2 - 4AC \geq 0$ and $B^2 - 4AC \geq 0$, respectively.

3) One can show that for $M_j > M_i$ and unpolarized incident electron beam ($P_e = 0$) $s_{2,3}$ fulfill the inequalities

$$M_j^2 - \frac{B}{A} < s_{2,3} < M_j^2\ . \tag{4.17}$$

4) Similarily, $S_{2,3}$ fulfill the inequality

$$S_{2,3} < -\frac{B}{A} < M_i^2 + M_j^2 \ . \tag{4.18}$$

5) (4.17) and (4.18) indicate that the region in $\sqrt{s}$ where the electroweak asymmetries show most structure lies essentially *below* the mass of the second vector boson.

6) The expressions for A, B and C greatly simplify if also V_j couples purely axial vector like to charged leptons and, moreover, is a narrow resonance ($\Gamma_j \ll M_j$). This, for example, happens sometimes for additional weak vector bosons in GUT's [23] or, as we shall see below, for the Y_L-boson if λ_Y^2 takes on a certain value. In this case both s_2 and s_3 exist and one finds:

$$s_2 = \frac{a_{ie}^2}{a_{ie}^2 + a_{je}^2} M_j^2 + \frac{a_{je}^2}{a_{ie}^2 + a_{je}^2} M_i^2 \ , \tag{4.19}$$

$$s_3 = M_j^2 \ . \tag{4.20}$$

If we identify V_i with the Z-boson, Eqs. (4.5) to (4.20) should hold to a very good approximation as long as the vector and/or the axial vector coupling constants of the additional massive vector boson are larger than $v_e = 1 - 4sin^2\theta_W \approx 0.08$ (for $sin^2\theta_W = 0.23$ corresponding to $M_Z = 92\ GeV$). This, for example, is the case in all GUT's, left-right symmetric or superstring inspired models where the coupling constants of the second vector bosons are typically of the order of the electromagnetic coupling constant e, or larger. It also holds true in the composite weak boson models we are considering. Since λ_Y^2 is bounded from above (see Eq. (3.9)), g_Y according to Eq. (3.4) has to be larger than about 0.35.

Comparing the number and the positions of the zeros in A_{FB} and A_{LR} in models with an additional massive vector boson V_j with the ones in the standard model (see Fig. 1 and Eqs. (2.22) and (2.33)), we observe that at least above the Z-pole and below $\sqrt{M_Z^2 + M_j^2}$ rather large deviations from the standard model may occur. This means that by measuring electroweak asymmetries at LEPII energies ($\sqrt{s} = 190\ GeV$) one actually may be sensitive to V_j-masses much larger than $\sqrt{s}$. Subsequently, we shall demonstrate this for the Y- and the Y_L-boson. In Section 5 we shall estimate lower limits on the Y- and Y_L-masses one should

be able to obtain from experiments at LEPI/SLC and LEPII, provided that no differences from the standard model asymmetries are observed.

4.2. Implications of Y and Y_L on Electroweak Asymmetries

Using Eqs. (4.1) - (4.3) it is now a straightforward exercise to calculate the electroweak asymmetries in the Y- and Y_L-case. The vector and axial vector coupling constants of the Z-boson, including the mixing effects with the $Y(Y_L)$-boson, are given in Eqs. (3.17) - (3.20). The coupling constants $V_{Y_{(L)}}$ and $A_{Y_{(L)}}$ of $Y(Y_L)$ were discussed in detail in [10]. For completeness, we recall here their form and summarize those properties of $V_{Y_{(L)}}$ and $A_{Y_{(L)}}$ which are relevant for our subsequent discussion.

The vector and axial vector coupling constants V_Y (V_{Y_L}) and A_Y (A_{Y_L}) of the $Y(Y_L)$-boson are given by

$$A_Y = \frac{e}{b_Y} \frac{M_Y^2}{M_Y^2 - m_Y^2} \frac{m_Y^2 - m_W^2}{M_Y^2 - m_W^2} T_3 \ , \tag{4.21}$$

$$V_Y = 2\frac{e}{b_Y} \frac{m_Y^2}{M_Y^2 - m_Y^2} Q - A_Y \ , \tag{4.22}$$

and

$$A_{Y_L} = -\frac{e}{b_Y} \frac{M_Y^2}{M_Y^2 - m_Y^2} Q + A_Y \ , \tag{4.23}$$

$$V_{Y_L} = -\frac{e}{b_Y}(1 - \frac{m_Y^2}{M_Y^2 - m_Y^2})Q - A_Y \ . \tag{4.24}$$

As shown in [10], $V_{Y_{(L)}}$ and $A_{Y_{(L)}}$ are rather sensitive to λ_Y^2. Inserting the expressions for b_Y (Eq.(3.6)) and m_Y^2 (Eq. (3.7)) into Eqs. (4.21) - (4.24) one finds that

i) for *small* values of λ_Y^2 , $Y(Y_L)$ couples almost exclusively to j_μ^Y ($j_\mu^{Y_L}$), and due to the vector dominance relation Eq. (3.4) the V's and A's become large for small λ_Y^2,

ii) for *large* λ_Y^2 the Y_L-boson couples almost purely *righthandedly* to fermions,

iii) for

$$\lambda_Y^2 = \frac{(1 - \lambda_W^2)M_Y^2 - m_W^2}{3M_Y^2 - 4m_W^2} \approx 0.26 \tag{4.25}$$

the Y_L-boson couples purely axial vector like to charged leptons (i.e. $V_{Y_L} = 0$). The numerical value in Eq. (4.25) applies for $M_Y \geq 300\ GeV$. In this region the zero in V_{Y_L} is almost independent of M_Y.

Using Eqs. (3.17), (3.18), (4.21) and (4.22) for the v's and a's in Eq. (4.3) in the Y-case, and (3.19), (3.20), (4.23) and (4.24) in the Y_L-case we have computed the electroweak asymmetries as a function of $\sqrt{s}$ for a variety of values for the two parameters M_Y and λ_Y^2 characterizing Y and Y_L. Since $e^+e^- \to \mu^+\mu^-$ is the most important channel for LEPI/II and SLC experiments, we have restricted ourselves to the asymmetries in this particular reaction. The Z- mass was chosen to be 92 GeV, which is very close to the central value measured by UA2 [24]. The shape of the asymmetry curves does not change if M_Z is varied by a few GeV. To compute Γ_Z and $\Gamma_{Y_{(L)}}$ we assumed that the t-quark mass fulfils the inequality $M_Z/2 < m_t \ll M_Y/2$, but our results are insensitive to the choice of this parameter. Finally, the detector acceptance x was fixed to be $x = 1$. For values $x < 1$ one has to rescale A_{FB} by a factor $4x/3 + x^2$ (A_{LR} is independent of x).

Our results are presented in Figs. 4 to 8. To illustrate the implications of Y and Y_L on the electroweak asymmetries, we have included the standard model tree-level prediction in each figure. Fig. 4 shows how the forward-backward asymmetry for an unpolarized electron beam ($P_e = 0$) and $M_Y = 500\ GeV$ changes with λ_Y^2. Curves of a similar shape are also obtained for different values of M_Y. It turns out that Y and Y_L affect A_{FB} in a rather different way. While the Y_L-boson reveals itself through a typical resonance structure, the presence of the Y-boson is signalled by a rather marked step which moves with increasing λ_Y^2 to higher values of $\sqrt{s}$. For $\sqrt{s} \leq M_Z$ the deviations from the standard model prediction are rather small. Above the Z-pole, however, the $Y(Y_L)$-influence is quite dramatic and large deviations from the standard model may occur already for $\sqrt{s} \ll M_Y$. For small (large) values of λ_Y^2 and $\sqrt{s} \to \infty$ the forward-backward asymmetry approaches values close to 3/4 in the Y_L-case, thereby reflecting the approximately lefthanded (righthanded) coupling of the Y_L. Fig. 4 also demonstrates the correctness of the general results derived in Section 4.1. For all three values of λ_Y^2 shown, A_{FB} has one zero in the Y- , and three zeros in the Y_L-case. Furthermore, one observes that the inequality (4.17) is satisfied and that Y and Y_L practically do not affect

the first zero in A_{FB}. In Fig. 4b the parameter λ_Y^2 has been tuned to the value in Eq. (4.25) where V_{Y_L} vanishes for charged leptons. In this case the resonance structure of Y_L in A_{FB} is maximally enhanced. Identifying the Y_L-boson with V_j from Section 4.1, Eqs. (4.19) and (4.20) are seen to be very well satisfied.

Fig. 5 illustrates the variation of A_{FB} with M_Y for fixed $\lambda_Y^2 = 0.2$ and $P_e = 0$. While the shape of the curves remain qualitatively the same, the values of $\sqrt{s}$ where A_{FB} is minimal, maximal or zero increase almost proportional with M_Y. The same effect also occurs for different values of λ_Y^2.

In Fig. 6 we compare the forward-backward asymmetry in the Y- and Y_L-case with $M_Y = 500\ GeV$ and $\lambda_Y^2 = 0.1$ for different values of P_e. If $\sqrt{s} \leq 150\ GeV$, A_{FB} is almost independent of P_e since $Y(Y_L)$- contributions are suppressed and, as we have noticed in Section 2, P_e-dependent Z-boson contributions are proportional to $v_e = 1 - 4sin^2\theta_W \approx 0.08$, and therefore small. At larger values of $\sqrt{s}$, however, the forward-backward asymmetry depends considerably on P_e. For values of M_Y and λ_Y^2 different from the ones chosen in Fig. 6 one finds in general a variation of A_{FB} with P_e similar to the one shown there. Only in the Y_L-case for $\lambda_Y^2 \approx 0.26$, the value where V_{Y_L} vanishes for charged leptons, A_{FB} is independent of P_e.

In Figs. 7 and 8 we present our results for A_{LR}/P_e. Fig. 7 illustrates how A_{LR}/P_e versus $\sqrt{s}$ behaves as a function of λ_Y^2. Again the $Y(Y_L)$-mass is 500 GeV, but similar curves are also obtained for other values of M_Y. For $\sqrt{s} > M_Z$, the left-right asymmetry in the Y- and Y_L-case in general differs substantially from the standard model prediction of A_{LR}. The presence of the Y-boson is signalled by a rather pronounced peak which with increasing λ_Y^2 is shifted towards higher values of $\sqrt{s}$. The Y_L-boson, on the other hand, affects A_{LR} in a completely different way. For small or large values of λ_Y^2 the appearance of the Y_L is characterized by a step where A_{LR} in general changes its sign. Due to the approximately lefthanded (righthanded) coupling of Y_L, A_{LR} approaches values close to +1 (-1) for small (large) λ_Y^2 and $\sqrt{s} \gg M_Y$. If the Y_L-boson couples purely axial vector like as in Fig. 7b ($\lambda_Y^2 \approx 0.26$), its influence on the left-right asymmetry is minimized and deviations from the standard model prediction are quite small. Identifying $Y_L = V_i$ we immediately see that Eq. (4.12) and the inequality (4.18) are satisfied.

Fig. 8, finally, shows the variation of A_{LR}/P_e with M_Y. The parameter λ_Y^2 was chosen to be 0.2, but for different values the results are quite similar. As one can see, increasing M_Y results in effects analogous to the ones observed for A_{FB} in Fig. 5. While the shape of the curves remains unchanged, the minima, maxima and zeros move almost proportional with M_Y to larger values of $\sqrt{s}$.

From Figs. 4 to 8 we recognize that in preon models containing an isoscalar weak vector boson $Y(Y_L)$ the electroweak asymmetries at LEPII energies may be significantly affected, even for values of M_Y as large as 1 TeV. In general, the influence of Y and Y_L will be quite different. By measuring A_{FB} and A_{LR} at LEPII (provided that the incident electron beam can be longitudinally polarized) one, therefore, will be sensitive to $Y(Y_L)$-masses much larger than $\sqrt{s}$. On the other hand, near the Z-peak the deviations are normally rather small. Since the Z-contribution is maximally enhanced at $\sqrt{s} \simeq M_Z$, $Y(Y_L)$-effects there arise predominantly from the influence of $Y(Y_L)$ on the Z-boson vector and axial vector coupling constants via its mixing with the photon (see Section 3.1). Nevertheless, due to the large counting rate at the Z-pole they should be observable if M_Y is in the few hundred GeV range. Alternatively, if no deviations from the standard model are seen at LEPI/SLC and LEPII, measurements of A_{FB} and A_{LR} in addition to M_Z, m_W/M_Z and $\Gamma(Z \to \ell^+\ell^-)$ will further constrain the $(\lambda_Y^2,\ M_Y)$ parameter space. Since Y and Y_L affect electroweak asymmetries at LEPII energies to a much larger extent than near the Z-pole, the most stringent bounds on M_Y and λ_Y^2 are expected to come from A_{FB} and A_{LR} measurements at LEPII. This will be discussed in more detail in the next Section.

5. Searching for Y and Y_L at LEP and SLC

We will now combine the results of the previous Sections in order to obtain restrictions on the (λ_Y^2, M_Y) parameter space which one can expect to result from experiments at LEPI/SLC and LEPII, provided that no deviations from the standard model are observed. Rather than performing a full numerical simulation, we shall carry out a somewhat simplified analysis and focus on the question which quantity may constrain λ_Y^2 and M_Y most efficiently. We start by briefly recalling present experimental limits on (λ_Y^2, M_Y). In the second part we shall discuss to

what extent m_W/M_Z and $\Gamma(Z \to \ell^+\ell^-)$ measurements may reduce the allowed λ_Y^2 and M_Y range. In Section 5.3 we consider bounds resulting from electroweak asymmetries and in Section 5.4, finally, we combine all constraints and derive lower limits on the $Y(Y_L)$-masses.

5.1. Constraints on (λ_Y^2, M_Y) From Present Experiments

Limits on λ_Y^2 and M_Y presently come from measurements of m_W and M_Z at the CERN $p\bar{p}$ collider [24] and from low energy lepton-hadron scattering experiments [25]. Data from neutrino-lepton scattering [25] and A_{FB} measurements at PEP and PETRA [26] are not yet accurate enough to yield sensible bounds.

According to Eqs. (3.7) and (3.10) the Z-boson mass is affected by the $Y(Y_L)$ photon mixing. Since M_Z decreases with increasing λ_Y^2, an upper limit on the $Y(Y_L)$ photon mixing parameter can be obtained from the present experimental values of the W- and Z-mass. Using Eqs. (3.7) and (3.10) together with the results of Ref. [24] we find $\lambda_Y^2 < 0.67$ (0.75) for $M_Y = 0.5\ TeV$ (1 TeV) which is slightly more restrictive than the bound (3.9) from the consistency condition $m_Y^2 \geq 0$.

Constraints far better than the ones from m_W and M_Z are provided by present low energy lepton-hadron scattering data [25]. Since the contributions of Y and Y_L to the effective low energy Lagrangian cannot be parametrized by ρ and $sin^2\theta_W$ (see e.g. [8]), we have to use the individual couplings $\epsilon(u_L)$ ($\epsilon(d_L)$) and $\epsilon(u_R)$ ($\epsilon(d_R)$) of left- and righthanded $u(d)$-quarks in order to obtain information about the allowed values of λ_Y^2 and M_Y. From the expressions derived for the ϵ's in Ref. [8] we observe that the $Y(Y_L)$-contributions to the couplings of the u- and d-quarks are either proportional to $1/m_Y^2$ or to $1/\lambda_Y^2\ m_Y^2$. These contributions become consequently obviously large for a small value of λ_Y^2 for the latter term whereas for both terms a large value of λ_Y^2 as well implies a bigger contribution to the couplings as $m_Y^2 \to 0$ for $\lambda_Y^2 \to \lambda_{Ymax}^2$ (cf. Eq. (3.7)). Therefore, for given M_Y the experimental results [25] for the couplings

$$\epsilon(u_L) = \ 0.344 \pm 0.026 \qquad \epsilon(d_L) = -0.419 \pm 0.022 \tag{5.1a}$$

$$\epsilon(u_R) = -0.153 \pm 0.022 \qquad \epsilon(d_R) = \ 0.076 \pm 0.041\ , \tag{5.1b}$$

lead to lower and upper bounds on λ_Y^2. Curves (1) and (2) in Fig. 9 (10) represent those bounds for the $Y(Y_L)$- boson and a Z-mass of 92 GeV. For M_Y

less than about 430 GeV no solution for λ_Y^2 compatible with (5.1) exists, but for $Y(Y_L)$-masses exceeding 500 GeV the allowed λ_Y^2 range is still very large (e.g. for $M_Y = 800\ GeV$: $0.035 \leq \lambda_Y^2 \leq 0.702$). Since $\epsilon(d_L)$ gives in general the most stringent bounds and the formulas for this quantity coincide in the Y- and Y_L- case, restrictions on λ_Y^2 from low energy lepton-nucleon scattering are rather similar for the Y- and the Y_L-boson. The limiting contour resulting from (5.1) depends, however, somewhat on the Z-mass chosen. Varying M_Z within the range of present experimental data [24] we obtain an absolute lower limit of about

$$M_Y > 370\ GeV \tag{5.2}$$

for the $Y(Y_L)$-mass which is somewhat more than what was found in Ref. [8]. The deviation can essentially be ascribed to the different experimental values of the ϵ's used here and in Ref. [8].

5.2. Restrictions from m_W/M_Z and $\Gamma(Z \to \ell^+\ell^-)$ Measurements

Once the Z-mass has been determined at LEPI and SLC, measurements of m_W/M_Z and the leptonic Z-width will provide new limits on M_Y and λ_Y^2 (or deviations from the standard model will show up). In order to estimate these limits we shall assume that the leptonic Z-width can be determined at LEPI/SLC with an accuracy of [14]

$$\frac{\delta\Gamma(Z \to \ell^+\ell^-)}{\Gamma(Z \to \ell^+\ell^-)} = 2\ \% \tag{5.3}$$

(see Section 2.3). For the experimental error in the ratio of W- and Z-masses we consider two different values. To demonstrate the importance of a precise measurement of m_W/M_Z we calculate limits resulting from this ratio for the error expected for ACOL (see Eq. (2.6)) as well as for the less optimistic one of

$$\delta(\frac{m_W}{M_Z}) = 1\ \% \ . \tag{5.4}$$

We identify the errors given in Eqs. (5.3), (5.4) and (2.6) with

$$\delta R = \mid R_{SM} \ - \ R_{Y_{(L)}} \mid \tag{5.5}$$

where R denotes either m_W/M_Z or $\Gamma(Z \to \ell^+\ell^-)$, and R_{SM} and $R_{Y_{(L)}}$ represent the corresponding predictions of the standard and the composite W-boson model

including leading log corrections, respectively. Assuming that no differences from the standard model appear in the m_W/M_Z and $\Gamma(Z \to \ell^+\ell^-)$ measurements and using Eqs. (2.4), (2.8) and (2.10) (with $\delta_\ell = 0$) we now convert the results of Figs. 2 and 3 into contours limiting the allowed range in the (λ_Y^2, M_Y) plane. Since deviations from the standard model grow for m_W/M_Z and the leptonic Z-width with increasing λ_Y^2 (see Section 3.2), we find from both quantities upper limits for the $Y(Y_L)$ photon mixing parameter. Curve (3a) and (3b) in Fig. 9 represent the upper bound on λ_Y^2 from m_W/M_Z in the Y-case for the error given in Eq. (2.6) and (5.4), respectively. The corresponding limits for the Y_L-boson are shown in Fig. 10. Curve (4) in Fig. 9 (10) gives the upper limit resulting from the leptonic Z-width for the $Y(Y_L)$. In each case a Z-mass of 92 GeV was employed, but our results do not change if M_Z is varied within the range allowed by present experimental data.

From Fig. 9 (10) we observe that if m_W/M_Z can be measured at ACOL or LEPI/II with an accuracy of 0.2 % it will give for $M_Y > 450$ GeV (550 GeV) the most stringent upper limit on λ_Y^2. The present upper limit (curve (2)) will be reduced by about a factor two. On the other hand, if the ratio of W- and Z-masses can be obtained only up to 1 %, a measurement of m_W/M_Z will only marginally improve the upper bound from present low energy lepton-hadron experiments. In this case a confirmation of the standard model prediction for $\Gamma(Z \to \ell^+\ell^-)$ within 2 % will already be more restrictive for λ_Y^2 (see Fig. 9 and 10). The upper limit resulting from the leptonic Z-width varies significantly with M_Y and for $Y(Y_L)$-masses less than 400 GeV (450 GeV) the deviation from the standard model is bigger than 2 % even for vanishing λ_Y^2. This is a reflection of the finiteness of δ (cf. Eq. (3.21)) in the limit $\lambda_Y^2 \to 0$.

5.3. Limits from Electroweak Asymmetries

Although m_W/M_Z and $\Gamma(Z \to \ell^+\ell^-)$ measurements at ACOL and LEPI/SLC may considerably reduce the allowed λ_Y^2 range, there will remain a substantial part of the (λ_Y^2, M_Y) plane which is still compatible with the data. High precision experiments at LEPI/SLC and LEPII determining the electroweak asymmetries may provide a further reduction of the allowed values of λ_Y^2 and M_Y. In order to see how useful the higher energy of LEPII and a longitudinally polarized e^--beam

will be, we shall now analyze for four different possible situations the constraints on the (λ_Y^2, M_Y) parameter space which would result if no deviations from the standard model forward-backward and left-right asymmetry are observed in the reaction $e^+e^- \to \mu^+\mu^-$:

a) Only $A_{FB}(\sqrt{s} = M_Z)$ with $P_e = 0$ can be measured. This corresponds to the situation where LEPII is not built and a longitudinally polarized e^--beam is not available at LEPI/SLC.

b) Both, $A_{FB}(\sqrt{s} = M_Z)$ and $A_{FB}(\sqrt{s} = 190\ GeV)$ with $P_e = 0$ are determined. This possibility would e.g. be realized if LEPII is built, but polarized beams are not available.

c) A_{FB} and A_{LR} can be measured at $\sqrt{s} = M_Z$ but not at higher values of $\sqrt{s}$. This would be the case if LEPII is not built, but a longitudinally polarized e^--beam can be achieved at LEPI/SLC.

d) A_{FB} and A_{LR} can both be determined at $\sqrt{s} = M_Z$ and $\sqrt{s} = 190\ GeV$. This could only be realized if LEPII is built and a polarized e^--beam would be available both at LEPI/SLC and LEPII.

Before we estimate the limits on (λ_Y^2, M_Y) in each of the four situations, we would like to discuss briefly radiative corrections to the electroweak asymmetries. The biggest contribution to these corrections will come from initial and final state bremsstrahlung radiation. Since this is a pure QED effect we expect that it will affect the electroweak asymmetries in the standard and the composite W-boson model in the same way. Moreover, these corrections turn out to be detector dependent [27] and we, therefore, shall assume for our subsequent analysis that the experimentalists will correct for this effect.

In Section 2.4 and 2.5 we have noted that in the standard model the purely weak corrections to A_{FB} and A_{LR} at the Z-peak constitute a sizeable fraction of the corresponding tree-level result and depend on the unknown quantities m_t and m_H. Varying m_t between 30 GeV and 180 GeV and m_H between 10 GeV and 1 TeV, A_{FB} and A_{LR} at $\sqrt{s} = M_Z$ change by as much as ± 0.01 and ± 0.02 depending somewhat on the Z-mass. Comparison with the expected experimental errors (cf. Eqs. (2.14) and (2.26)) shows that the variation of the weak corrections is significantly larger than $\delta A_{FB}(M_Z)$ and $\delta A_{LR}(M_Z)$. Measuring the forward-

backward and left-right asymmetry at the Z-pole one, therefore, is in the standard model sensitive to the t-quark and the Higgs-boson mass. From the point of view of testing the standard model versus a composite structure of the weak interactions this sensitivity, however, is not an advantage. Since the weak corrections to A_{FB} and A_{LR} arise beyond the leading log level and the effective Lagrangian theory we use to describe composite W-boson interactions is nonrenormalizable, we have no way of properly treating these corrections in the preon model.

To estimate limits on λ_Y^2 and M_Y from the electroweak asymmetries at $\sqrt{s} = M_Z$ we, therefore, adopt the following procedure. A_{FB} and A_{LR} are both, in the standard and in the composite W-boson model, treated at the leading log level. The standard model prediction for the electroweak asymmetries is not fully determined due to the variation of the purely weak corrections with m_t and m_H. This leads to a "theoretical" uncertainty which should be superimposed on the possible experimental errors. Since the uncertainty is much larger than the expected experimental errors (cf. Eqs. (2.14) and (2.26)), the combined errors will essentially coincide with the "theoretical" ones and consequently we shall use

$$\delta A_{FB}(M_Z) = 0.01 \quad , \quad \delta A_{LR}(M_Z) = 0.02 \tag{5.6}$$

in our subsequent analysis. At LEPII energies the purely weak corrections to A_{FB} and A_{LR} are less important than at $\sqrt{s} = M_Z$. This can be traced to the fact that the zeroth-order contribution at $\sqrt{s} = 190\ GeV$ is, in contrast to $\sqrt{s} = M_Z$, not suppressed by the small factor $v_e = 1 - 4sin^2\theta_W$ (see Eqs. (2.21) and (2.32)), whilst the radiative corrections contain in both cases contributions of $O(\alpha/(\pi sin^2\theta_W))$ not inhibited by v_e. For the errors in A_{FB} and A_{LR} at LEPII energies we, therefore, shall use the values given in Eqs. (2.15) and (2.27).

Identifying R in Eq. (5.5) with any of the asymmetries and assuming that no deviations from the standard model appear in asymmetry measurements at LEPI/SLC and LEPII we now obtain with Eqs. (2.16 - 18), (2.28 - 30) and the results from Section 3 and 4 the boundaries limiting the allowed range of the (λ_Y^2, M_Y) plane. Our results for the $Y(Y_L)$-boson are displayed in Fig. 11 (12). The labels attached to the plots refer to the corresponding situation a) to d) and the detector acceptance was always assumed to be complete ($x = 1$).

From Fig. 11a and 12a we observe that a measurement of $A_{FB}(\sqrt{s} = M_Z)$

with unpolarized beams in general results in a lower and an upper limit on λ_Y^2. The lower bound can be easily understood by remembering that, according to Eq. (3.4), the $Y(Y_L)$-boson coupling constant g_Y sharply increases with decreasing λ_Y^2. If the $Y(Y_L)$ photon mixing parameter is too small the $Y(Y_L)$-contribution to $A_{FB}(\sqrt{s} = M_Z)$ dominates over the Z-term and the difference from the standard model value becomes larger than 0.01. The upper limit originates mainly from the increasing deviation of the vector and the axial vector coupling constant of the Z-boson with growing λ_Y^2 from the corresponding standard model prediction. Comparing Fig. 11a and 12a with 11b and 12b, respectively, we see that the region in the (λ_Y^2, M_Y) plane which is not excluded shrinks considerably if the forward-backward asymmetry is also measured at $\sqrt{s} = 190\ GeV$. This is just a reflection of the sensitivity of A_{FB} above the Z-pole to values of M_Y much larger than $\sqrt{s}$. The narrow strips of allowed λ_Y^2 values in Fig. 11b and 12b result from an accidental coincidence of the standard and the composite W-boson model values of A_{FB} at $\sqrt{s} = M_Z$ and $\sqrt{s} = 190\ GeV$. Going from Fig. 11a and 12a to 11c and 12c one recognizes that the restrictions on λ_Y^2 become also more pronounced if in addition to $A_{FB}(\sqrt{s} = M_Z)$ A_{LR} can be measured at the Z-peak. However, the improvement is clearly less significant than for the case displayed in Fig. 11b (12b). While the upper bound is significantly reduced over the whole M_Y range in the Y_L-case, the lower limit is considerably strengthened for $M_Y < 650\ GeV$ in the Y-case. From Fig. 11d and 12d we, finally, observe that the allowed region in the (λ_Y^2, M_Y) plane can be most efficiently restricted if both, A_{FB} and A_{LR}, are determined at the Z-pole and at LEPII energies. Comparison of Fig. 11d (12d) with 11c (12c) demonstrates the usefulness of the higher LEPII energy in reducing the (λ_Y^2, M_Y) region not excluded by experimental data, whereas from Fig. 11b (12b) and 11d (12d) the advantage of a longitudinally polarized e^--beam, especially at LEPII energies, becomes apparent. Due to the sensitivity of A_{LR} above the Z-peak to values of M_Y much bigger than $\sqrt{s}$ the allowed region of the (λ_Y^2, M_Y) plane shrinks considerably if a polarized e^--beam can be achieved for LEPII and the left-right asymmetry can be measured.

For our analysis we have assumed that the electroweak asymmetries will be determined either at $\sqrt{s} = M_Z$ or at $\sqrt{s} = 190\ GeV$. At LEPI/SLC, however, a measurement of A_{FB} and/or A_{LR} in a whole range of a few GeV around the Z-

pole will be possible and one might wonder whether this could lead to considerably more stringent bounds than a determination of the electroweak asymmetries just at the Z-peak. It turns out that this is not the case. Since the deviations in A_{FB} and A_{LR} from the standard model are rather small around $\sqrt{s} = M_Z$ (see Figs. 4 to 8 and Section 4.2) and as the counting rate sharply drops once on is moving away from the Z-pole, one does not gain very much from such a measurement. The situation may, however, be completely different in the LEPII case. If LEPII could be operated also at $\sqrt{s}$ values sufficiently different from the designed one of 190 GeV and A_{FB} and A_{LR} could be determined, the sensitivity of the electroweak asymmetries above the Z-pole to values of M_Y much larger than $\sqrt{s}$ may lead to a further significant improvement of the bounds on λ_Y^2 and M_Y.

5.4. Lower Limits on M_Y from LEP and SLC Experiments

Finally, we may combine the bounds from present low energy lepton-hadron experiments, from m_W/M_Z and $\Gamma(Z \to \ell^+\ell^-)$ measurements and from electroweak asymmetries. The resulting lower limits on M_Y for each of the four situations discussed in Section 5.3 are presented in Table 1.

In situation a), where $A_{FB}(\sqrt{s} = M_Z)$ is the only asymmetry which is determined, we find that the bounds from electroweak asymmetries are in general *weaker* than the ones resulting from m_W/M_Z and $\Gamma(Z \to \ell^+\ell^-)$. The lower limits on M_Y, therefore, can be directly read off from Figs. 9 and 10. If we compare them with the present lower bound of $M_Y > 370$ GeV (cf. (5.2)) we see that if LEPII is not built and a longitudinally polarized e^--beam is not available at LEPI/SLC the lower limit can only slightly be improved at future e^+e^- colliders. Furthermore, we observe that the bound on M_Y in this case is almost independent from the accuracy of the m_W/M_Z measurement.

The lower limits on M_Y can be significantly strengthened if LEPII is built and, consequently, $A_{FB}(\sqrt{s} = 190\ GeV)$ can be determined (situation b)). For the Y-boson the most restrictive upper and lower bound on λ_Y^2 then results from m_W/M_Z or the leptonic Z-width, and the forward-backward asymmetry, respectively. In the Y_L-case, on the other hand, the contour limiting the allowed region of the (λ_Y^2, M_Y) plane almost exclusively comes from A_{FB} measurements at $\sqrt{s} = M_Z$ and $\sqrt{s} = 190\ GeV$, and the lower limit on M_Y, therefore, is independent of the

precision achieved for m_W/M_Z.

If instead of $A_{FB}(\sqrt{s} = 190\ GeV)$ the left-right asymmetry at the Z-peak can be determined, i.e. LEPII is not built, but a polarized e^--beam can be achieved for LEPI/SLC (situation c)), the bounds obtained for situation a) can only in the Y-case be improved somewhat. The allowed region of the (λ_Y^2, M_Y) plane is only slightly reduced by A_{FB} and A_{LR} measurements at $\sqrt{s} = M_Z$. For the Y_L-boson the upper limit from the electroweak asymmetries almost coincides with the one from m_W/M_Z if this ratio can be measured with an accuracy of 0.2 %.

The most restrictive lower bounds on M_Y can be found if A_{FB} and A_{LR} both can be measured at the Z-pole and at LEPII energies (situation d)). If m_W/M_Z can be determined with an accuracy of 0.2 % $Y(Y_L)$-masses less than 1.0 TeV (0.9 TeV) can be excluded. The allowed areas in the (λ_Y^2, M_Y) plane for this case are shown in Fig. 13. From Fig. 13a we observe that for the Y-boson the upper and lower limit on λ_Y^2 result from m_W/M_Z and electroweak asymmetry measurements, respectively. The bound on M_Y, therefore, depends somewhat on the precision which can be achieved for the ratio of W- and Z-masses. If m_W/M_Z can be obtained only with 1 % error, the lower limit on M_Y is reduced to 830 GeV. For the Y_L-boson, on the other hand, the limiting contour exclusively results from the electroweak asymmetries (see Fig. 13b) and the bound on M_Y is independent from the accuracy in the m_W/M_Z determination.

Comparing the limits on M_Y for situation a) to d) (cf. Table 1) we see that at LEPI/SLC even with a longitudinally polarized e^--beam *at best* $Y(Y_L)$-masses less than 600 GeV (500 GeV) can be excluded. These values could only then be significantly improved if the errors (5.6) for the forward-backward and the left-right asymmetry at the Z-peak, which are mainly due to the theoretical uncertainty of the standard model prediction for $A_{FB}(\sqrt{s} = M_Z)$ and $A_{LR}(\sqrt{s} = M_Z)$, could be considerably reduced.

If LEPII is built, the lower bound on M_Y can be improved up to 1 TeV and the most severe restrictions on λ_Y^2 arise in general from measurements of A_{FB} and A_{LR} at LEPII energies.

6. Conclusions

In this paper we have analyzed the implications of isoscalar weak vector bosons Y and Y_L on measurable quantities at future e^+e^- colliders. The Y and Y_L are coupled to the weak hypercharge current and its lefthanded part, respectively, and such particles typically appear in preon models with a composite structure of the weak interactions.

After a discussion of the relevant observables and their standard model predictions, we have developed an effective Lagrangian formalism to describe composite weak vector boson interactions. We also derived the expression for the Z-mass and the Lagrangian for interactions of the Z-boson with quarks and leptons in the presence of Y and Y_L, and analyzed how they affect the observable quantities m_W/M_Z and $\Gamma(Z \to \ell^+\ell^-)$.

In Section 4 the electroweak asymmetries were considered in detail. In the first part we presented the tree-level expressions for A_{FB} and A_{LR} for the general case of two massive vector bosons with arbitrary vector and axial vector coupling constants and discussed the location of zeros of the electroweak asymmetries which are useful in order to gain information about the shape of A_{FB} and A_{LR} versus $\sqrt{s}$ in the two vector boson case. Our results can be applied to any model with additional weak vector bosons, e.g. GUT's, left-right symmetric or superstring inspired models.

In the second part we studied the asymmetries in the Y- and Y_L-case, and illustrated the results of the general analysis in the first part.

Finally, in Section 5 we obtained restrictions on the (λ_Y^2, M_Y) parameter space which one can expect to result if experiments at LEP and SLC agree with the standard model predictions within the possible experimental accuracies.

Our results can be summarized as follows:

i) The ratio m_W/M_Z is affected in the same way by Y and Y_L and is always larger than in the standard model (see Fig. 2). Deviations from the standard model increase (decrease) with increasing λ_Y^2 (M_Y).

ii) On the other hand, Y and Y_L influence the leptonic Z-width in a completely different way: While $\Gamma(Z \to \ell^+\ell^-)$ in the Y-case is larger than in the stan-

dard model, the contrary is true for the Y_L-boson (see Fig. 3)

iii) For any model containing two massive neutral vector bosons there are at most three zeros in A_{FB} and A_{LR}. If one of the vector bosons couples (almost) axial vector like to charged leptons, as it is the case for the Z-boson, the first zero is (almost) unaffected by the existence of the second massive vector boson. The two other zeros, if they exist, are bounded from above in this case (see (4.17-18)).

iv) At $\sqrt{s}$ values below and around the Z-mass Y and Y_L affect A_{FB} and A_{LR} only slightly. Above the Z-peak, however, the electroweak asymmetries are rather sensitive to the presence of isoscalar weak vector bosons. At LEPII energies large deviations from the standard model predictions may occur even for $Y(Y_L)$-masses much larger than $\sqrt{s}$ (see Figs. 4 to 8).

v) If experiments at LEP and SLC agree with the standard model within the possible experimental accuracies, the region of the (λ_Y^2, M_Y) plane which is compatible with present data will be strongly reduced (see Figs. 9 to 13). With LEPI/SLC $Y(Y_L)$-masses up to 600 GeV (500 GeV) can be excluded. Due to the sensitivity of the electroweak asymmetries above the Z-pole to values of M_Y much larger than $\sqrt{s}$, the lower limit on M_Y may be pushed up to 1 TeV at LEPII (if a longitudinally polarized e^--beam can be realized at LEPII).

Our results clearly demonstrate the usefulness of the higher LEPII energy and of a polarized incident electron beam in searching for Y and Y_L. Since isoscalar weak vector bosons in preon models with composite W- and Z-bosons are expected to have a mass of the order of a few hundred GeV, many models of this type would be excluded if one could place a lower bound of 1 TeV on the $Y(Y_L)$-masses. Our analysis shows that this limit can be reached with LEPII but not with LEPI/SLC unless the errors $\delta A_{FB}(\sqrt{s} = M_Z)$ and $\delta A_{LR}(\sqrt{s} = M_Z)$ can be significantly reduced. This, however, will be difficult since as we have seen in Section 5.3, the dominant uncertainty arises from the conceptual difficulty of comparing the fully renormalizable standard model with an effective theory in which only leading log corrections can be included.

The analysis performed in this paper can easily be repeated for any other

model containing a second massive weak vector boson. The main difference to the $Y(Y_L)$-case are the different vector and axial vector coupling constants. In view of the results for the general two vector boson case obtained in Section 4.1 for the electroweak asymmetries, we in general expect large deviations in A_{FB} and A_{LR} from the standard model at LEPII energies. If asymmetry measurements agree with the standard model predictions at LEPII strong limits on the mass and/or the coupling constant will not only be obtainable for Y and Y_L but also for excited Z-bosons [28] in composite weak boson models, or additional massive neutral vector bosons appearing in GUT's, left-right symmetric models, superstring inspired models etc. Our results may, therefore, at least qualitatively be valid in a more general context.

ACKNOWLEDGEMENTS

We would like to thank the members of the working group on compositeness of the LEP200 Workshop, in particular A. Blondel, B. Schrempp, F. Schrempp and D. Treille for useful and stimulating discussions. We are also grateful to A. Sirlin for helpful comments. One of us (U.B.) would like to acknowledge financial support of the Max-Kade-Foundation, New York.

REFERENCES

[1] S.L. Glashow, *Nucl. Phys.* **22** (1961) 579;
S. Weinberg, *Phys. Rev. Lett.* **19** (1967) 1264;
A. Salam, Proc. 8th Nobel Symposium, ed. N. Svartholm, Almquist and Wiksells, Stockholm 1968, p. 367.

[2] UA1 collaboration, G. Arnison et al., CERN-EP/85-185 (1985) preprint;
UA2 collaboration, J.A. Appel et al., *Z. Phys.* **C30** (1986) 1.

[3] For a review see e.g. W. Buchmüller, *Acta Physica Austriaca, Suppl.* **XXVII** (1985) 517.

[4] R. Kögerler and D. Schildknecht, CERN-TH 3231 (1982) (unpublished);
H. Fritzsch, R. Kögerler and D. Schildknecht, *Phys. Lett.* **114B** (1982) 157;
B. Schrempp and F. Schrempp, DESY 84-055 (1984) (unpublished).

[5] M. Kuroda and D. Schildknecht, *Phys. Lett.* **121B** (1983) 173;
U. Baur, D. Schildknecht and K.H. Schwarzer, MPI-PAE/PTh 29/85 (1985), to appear in *Phys. Rev. D* (Jan. 1987).

[6] S.F. King and S.R. Sharpe, *Nucl. Phys.* **B253** (1985) 1;
U. Baur and K.H. Streng, *Z. Phys.* **C30** (1986) 325.

[7] W. Buchmüller, *Phys. Lett.* **145B** (1984) 151.

[8] M. Kuroda, D. Schildknecht and K.H. Schwarzer, *Nucl. Phys.* **B261** (1985) 432.

[9] C. Korpa and Z. Ryzak, *Phys. Rev.* **D34** (1986) 2139.

[10] U. Baur and K.H. Schwarzer, *Phys. Lett.* **180B** (1986) 163.

[11] R.W. Robinett and J.L. Rosner, *Phys. Rev.* **D25** (1982) 3036.

[12] M. Cvetic and B.W. Lynn, SLAC-PUB-3900 (1986) preprint.

[13] J.P. Ader, S. Narison and J.C. Wallet, *Phys. Lett.* **176B** (1986) 215;
P.J. Franzini and F.J. Gilman, SLAC-PUB-3932 (1986) preprint.

[14] G. Altarelli, in: "Physics at LEP", CERN Yellow Report 86/02 (1986), Vol. 1, ed. J. Ellis and R.D. Peccei.

[15] See e.g. W.J. Marciano and A. Sirlin, *Phys. Rev.* **D29** (1984) 945 and references therein.

[16] See e.g. D. Yu. Bardin, S. Riemann and T. Riemann, *Z. Phys.* **C32** (1986) 121 and references therein.

[17] G. Barbiellini et al., in "Physics at LEP", CERN Yellow Report 86/02 (1986), Vol. 2, ed. J. Ellis and R.D. Peccei.

[18] A. Blondel, private communication.

[19] B.W. Lynn and R.G. Stuart, *Nucl. Phys.* **B253** (1985) 216;
B.W. Lynn, M.E. Peskin and R.G. Stuart, in "Physics at LEP", CERN Yellow Report 86/02 (1986), ed. J. Ellis and R.D. Peccei.

[20] P.Q. Hung and J.J. Sakurai, *Nucl. Phys.* **B143** (1978) 81;
J.D. Bjorken, *Phys. Rev.* **D19** (1979) 335.

[21] L. Hall, *Nucl. Phys.* **B178** (1981) 75;
S. Dawson, J.S. Hagelin and L. Hall, *Phys. Rev.* **D23** (1981) 2666.

[22] T.D. Lee, *Phys. Rev.* **168** (1968) 1714.

[23] P. Langacker, R.W. Robinett and J.L. Rosner, *Phys. Rev.* **D30** (1984) 1470.

[24] G. Altarelli, talk given at the 23rd Int. Conf. on High Energy Physics, Berkeley, USA, July 16 - 23, 1986 and Rome preprint n. 529 (1986).

[25] G. Barbiellini and C. Santoni, CERN-EP/85-117 (1985) preprint.

[26] B. Naroska, talk given at the 21st. Recontré de Moriond, Les Arcs, France, March 9-16, 1986 and DESY 86-051 preprint.

[27] F.A. Berends and R. Kleiss, *Nucl. Phys.* **B177** (1981) 237;
F.A. Berends, R. Kleiss and S. Jadach, *Nucl. Phys.* **B202** (1982) 63;
M. Böhm and W. Hollik, *Nucl. Phys.* **B204** (1982) 45.

[28] U. Baur, M. Lindner and K.H. Schwarzer, in preparation

Table 1

Situation	a	b	c	d
Y-boson	460 (450)	720 (560)	600 (530)	1010 (830)
Y_L-boson	500 (500)	880 (880)	500 (500)	880 (880)

Lower bounds on M_Y (in GeV) resulting from a combination of the constraints from present low energy lepton-nucleon data, a measurement of m_W/M_Z with 0.2 % error and $\Gamma(Z \to \ell^+\ell^-)$ with 2 % error, and from electroweak assymmetries. Numbers in parentheses apply if the ratio of W- and Z- masses can be obtained only with a precision of 1.0 %.

FIGURE CAPTIONS

1. The standard model forward-backward asymmetry $A_{FB}^{e^+e^-\to\mu^+\mu^-}$ for unpolarized beams and ideal detector acceptance ($x = 1$) and the standard model left-right asymmetry $A_{LR}^{e^+e^-\to\mu^+\mu^-}/P_e$ (P_e: degree of longitudinal polarization of the incident electron beam) versus $\sqrt{s}$. The Z-mass was chosen to be 92 GeV. In the lower right corner a close-up of the region near the Z-pole is shown.

2. The ratio m_W/M_Z versus M_Z in presence of the isoscalar boson Y or Y_L (solid lines)
   a) for $M_Y = 500\ GeV$, $\lambda_Y^2 = 0.2,\ 0.4,\ 0.6$;
   b) for $\lambda_Y^2 = 0.2$, $M_Y = 300,\ 500,\ 800,\ 1000\ GeV$.
   The numbers attached to the curves denote the values of λ_Y^2 and M_Y (in GeV), respectively. The dashed line represents the standard model prediction.

3. The leptonic Z-width $\Gamma(Z \to \ell^+\ell^-)$ versus M_Z in presence of the isoscalar boson Y (solid lines) and Y_L (dotted lines)
   a) for $M_Y = 500\ GeV$, $\lambda_Y^2 = 0.0,\ 0.2,\ 0.6$;
   b) for $\lambda_Y^2 = 0.2$, $M_Y = 500,\ 800,\ 1000\ GeV$.
   On the curves the corresponding values of λ_Y^2, respectively M_Y (in GeV) are shown. The dashed line represents the standard model prediction.

4. The forward-backward asymmetry $A_{FB}^{e^+e^-\to\mu^+\mu^-}$ for unpolarized electron beam ($P_e = 0$) and ideal detector acceptance ($x = 1$) in the $Y(Y_L)$-case (dashed (dotted) line) for $M_Y = 500\ GeV$ and
   a) $\lambda_Y^2 = 0.1$,
   b) $\lambda_Y^2 = 0.26$,
   c) $\lambda_Y^2 = 0.5$.
   The solid line represents the standard model prediction. The Z-mass was chosen to be 92 GeV.

5. The forward-backward asymmetry $A_{FB}^{e^+e^-\to\mu^+\mu^-}$ for unpolarized electron beam ($P_e = 0$) and ideal detector acceptance ($x = 1$) in the $Y(Y_L)$-

case (dashed (dotted) lines) for $\lambda_Y^2 = 0.2$ and $M_Y = 500\ GeV$ and $M_Y = 1\ TeV$, respectively. The numbers attached to the curves denote the $Y(Y_L)$-mass in GeV. The solid line represents the standard model prediction. The Z-mass was chosen to be 92 GeV.

6. The forward-backward asymmetry $A_{FB}^{e^+e^-\to\mu^+\mu^-}$ for ideal detector acceptance ($x = 1$), $\lambda_Y^2 = 0.1$, $M_Y = 500\ GeV$ and $P_e = 0$ (solid line), $P_e = 0.5$ (dashed line) and $P_e = 1$ (dotted line)
   a) in the Y-case,
   b) in the Y_L-case.
   For the Z-mass we used 92 GeV.

7. The left-right asymmetry $A_{LR}^{e^+e^-\to\mu^+\mu^-}/P_e$ in the $Y(Y_L)$-case (dashed (dotted) line) for $M_Y = 500\ GeV$ and
   a) $\lambda_Y^2 = 0.1$,
   b) $\lambda_Y^2 = 0.26$,
   c) $\lambda_Y^2 = 0.5$.
   The solid line represents the standard model prediction. The Z- mass is 92 GeV.

8. The left-right asymmetry $A_{LR}^{e^+e^-\to\mu^+\mu^-}/P_e$ in the $Y(Y_L)$-case (dashed (dotted) lines) for $\lambda_Y^2 = 0.2$ and $M_Y = 500\ GeV$ and $M_Y = 1\ TeV$, respectively. On the curves the corresponding values of M_Y (in GeV) are shown. The solid line gives the standard model prediction. For the Z- mass we used 92 GeV.

9. Lower and upper limits on λ_Y^2 versus M_Y in the Y-case. Curves (1) and (2) represent the lower and upper limit from present low energy lepton-nucleon experiments, respectively. Curves (3) and (4) show the upper limits which would result from measurements of m_W/M_Z and $\Gamma(Z \to \ell^+\ell^-)$ with
   a) 0.2% error (curve (3a))
   b) 1.0% error (curve (3b))
   in m_W/M_Z and 2% error in the leptonic Z-width. The Z-mass was chosen to be 92 GeV.

10. The same as in Fig. 9 for the Y_L-case.

11. Contours limiting the allowed λ_Y^2 and M_Y range which result from a measurement of
    a) $A_{FB}(\sqrt{s} = M_Z)$ with 1 % error,
    b) $A_{FB}(\sqrt{s} = M_Z)$ and $A_{FB}(\sqrt{s} = 190\ GeV)$ with 1 % and 3 % error, respectively,
    c) $A_{FB}(\sqrt{s} = M_Z)$ and $A_{LR}(\sqrt{s} = M_Z)$ with 1 % and 2 % error, respectively,
    d) A_{FB} and A_{LR} at both $\sqrt{s} = M_Z$ and $\sqrt{s} = 190\ GeV$ with the corresponding errors from a), b) or c)
    in the Y-case. The hatched side of the boundary curves indicates the allowed region. For the Z-mass we used 92 GeV.

12. The same as in Fig. 11 for the Y_L-case.

13. Allowed regions in the (λ_Y^2, M_Y) plane (hatched areas) resulting from a combination of the lower (curve(1)) and upper limits (curve(2)) from present lepton-hadron scattering data, the upper bounds from a measurement of m_W/M_Z with 0.2 % error (curve (3)) and $\Gamma(Z \to \ell^+\ell^-)$ with 2 % error (curve (4)), and the limiting contour from A_{FB} and A_{LR} measurements at $\sqrt{s} = M_Z$ and $\sqrt{s} = 190\ GeV$ (curve (5))
    a) for the Y-boson,
    b) for the Y_L-boson.
    The Z-mass was chosen to be 92 GeV.

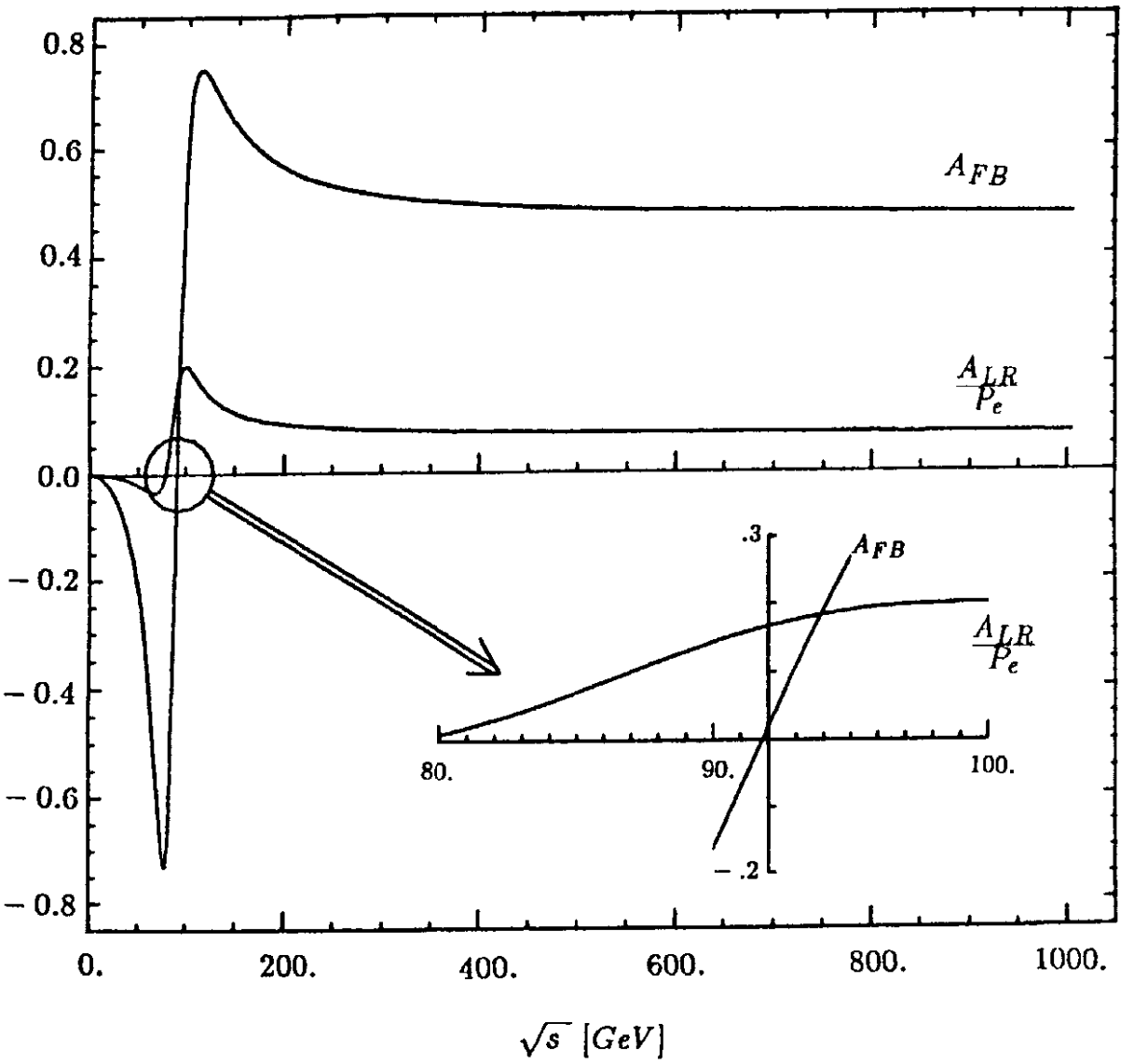
0.8
0.6
0.4
0.2
0.0
−0.2
−0.4
−0.6
−0.8
0.
200.
400.
600.
800.
1000.
A_{FB}
$\frac{A_{LR}}{P_e}$
.3
−.2
80.
90.
100.
$\sqrt{s}$ [GeV]

Fig. 1

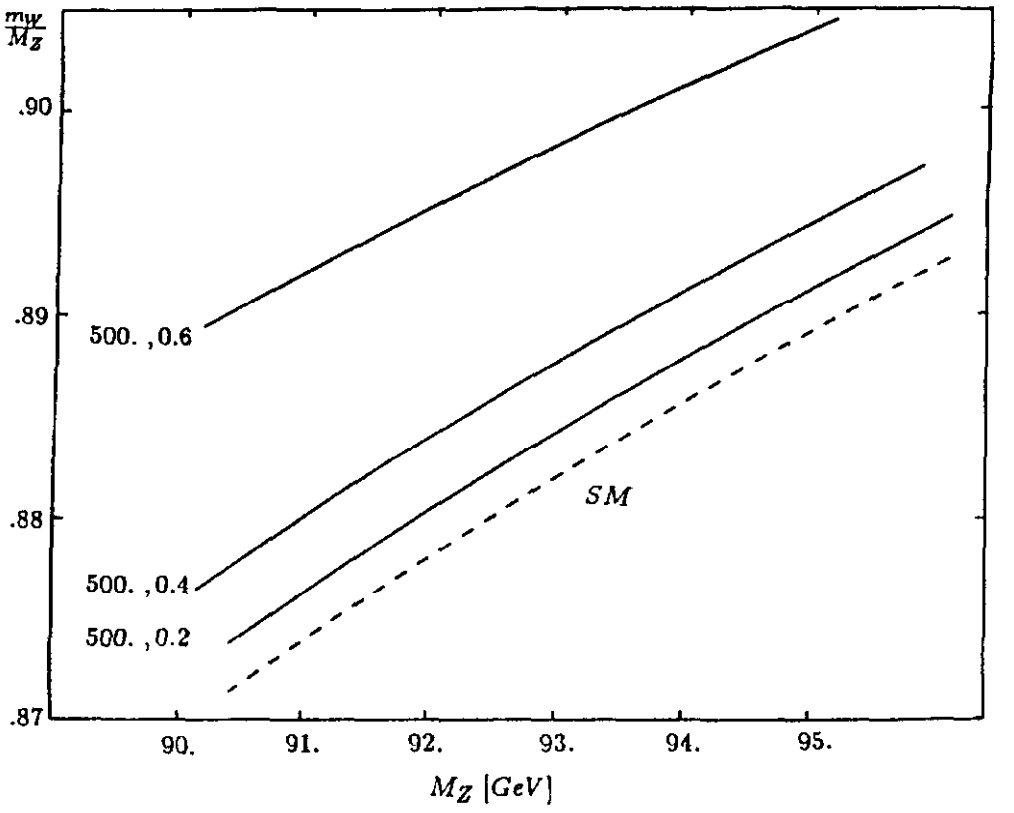
$\frac{m_W}{M_Z}$
.90
.89
.88
.87
500. , 0.6
500. , 0.4
500. , 0.2
SM
90.
91.
92.
93.
94.
95.
M_Z [GeV]

Fig. 2a

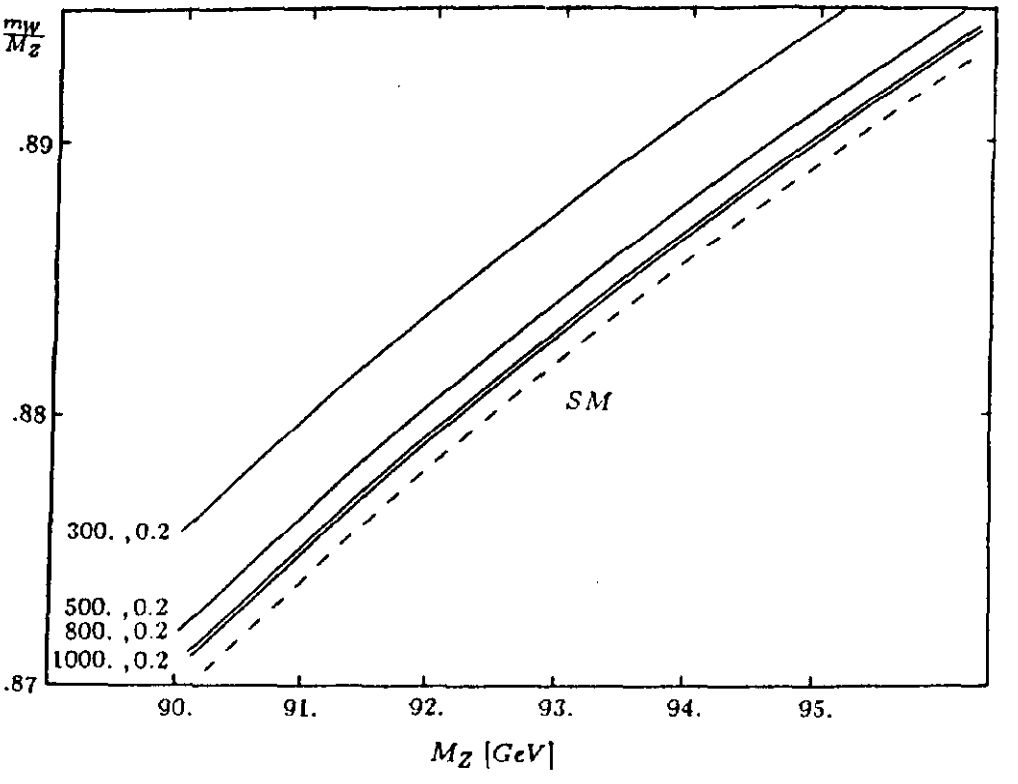
$\frac{m_W}{M_Z}$
.89
.88
.87
300. , 0.2
500. , 0.2
800. , 0.2
1000. , 0.2
SM
90.
91.
92.
93.
94.
95.
M_Z [GeV]

Fig. 2b

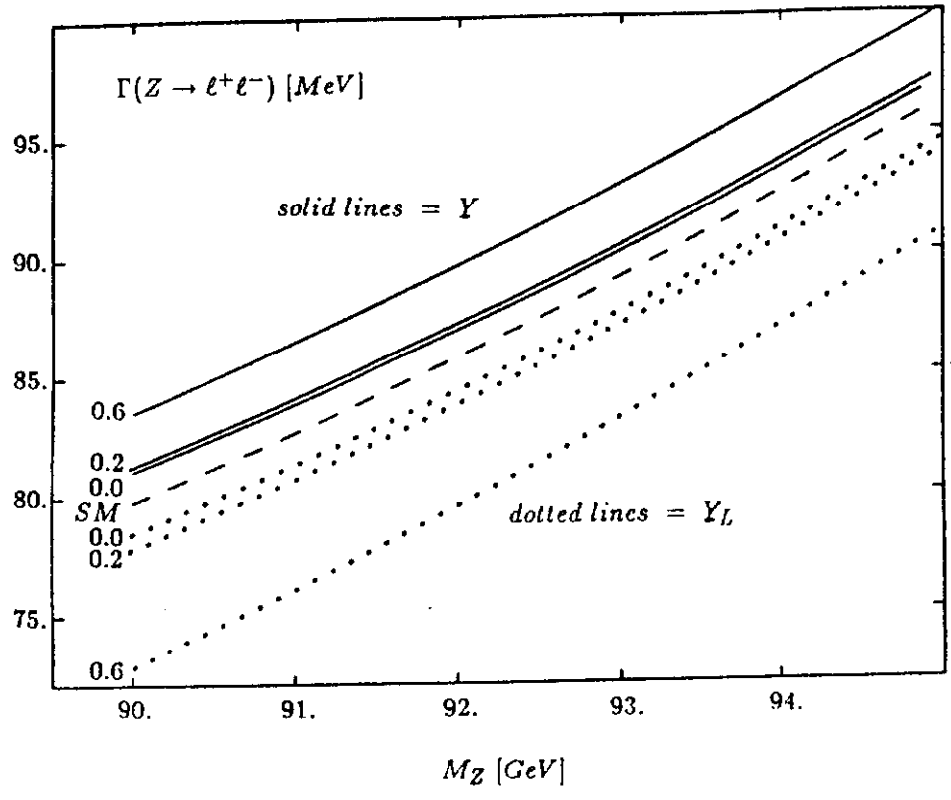
$\Gamma(Z \to \ell^+\ell^-)$ [MeV]
95.
90.
85.
80.
75.
solid lines = Y
dotted lines = Y_L
0.6
0.2
0.0
SM
0.0
0.2
0.6
90.
91.
92.
93.
94.
M_Z [GeV]

Fig. 3a

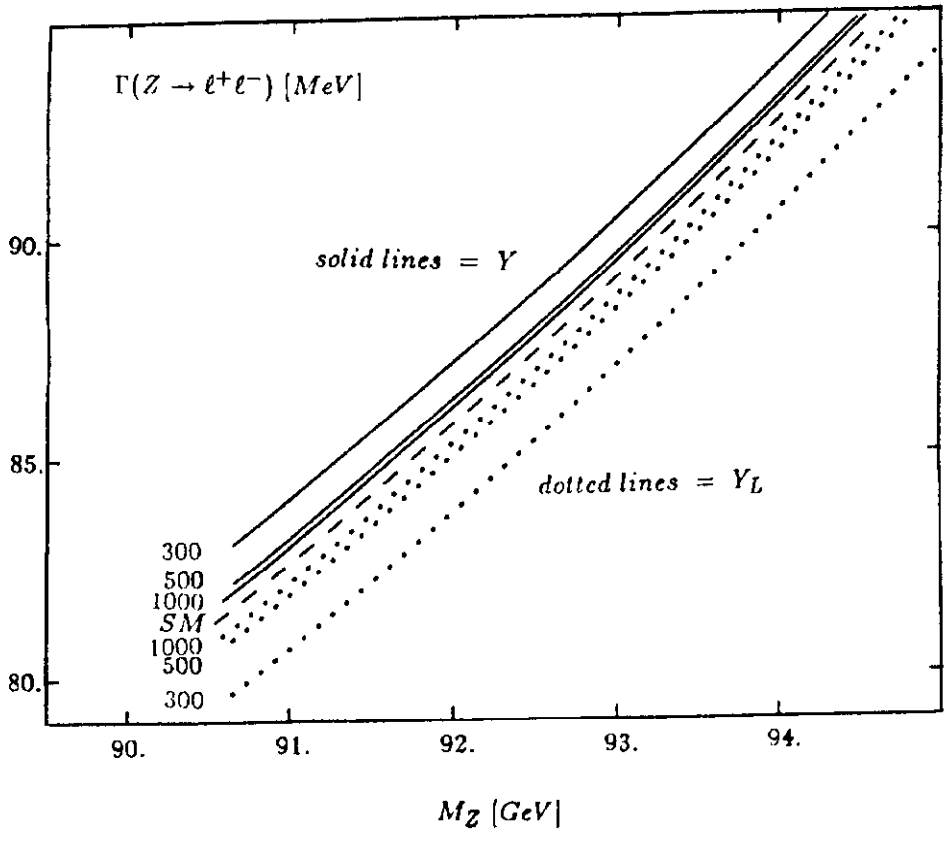
$\Gamma(Z \to \ell^+\ell^-)$ [MeV]
90.
85.
80.
solid lines = Y
dotted lines = Y_L
300
500
1000
SM
1000
500
300
90.
91.
92.
93.
94.
M_Z [GeV]

Fig. 3b

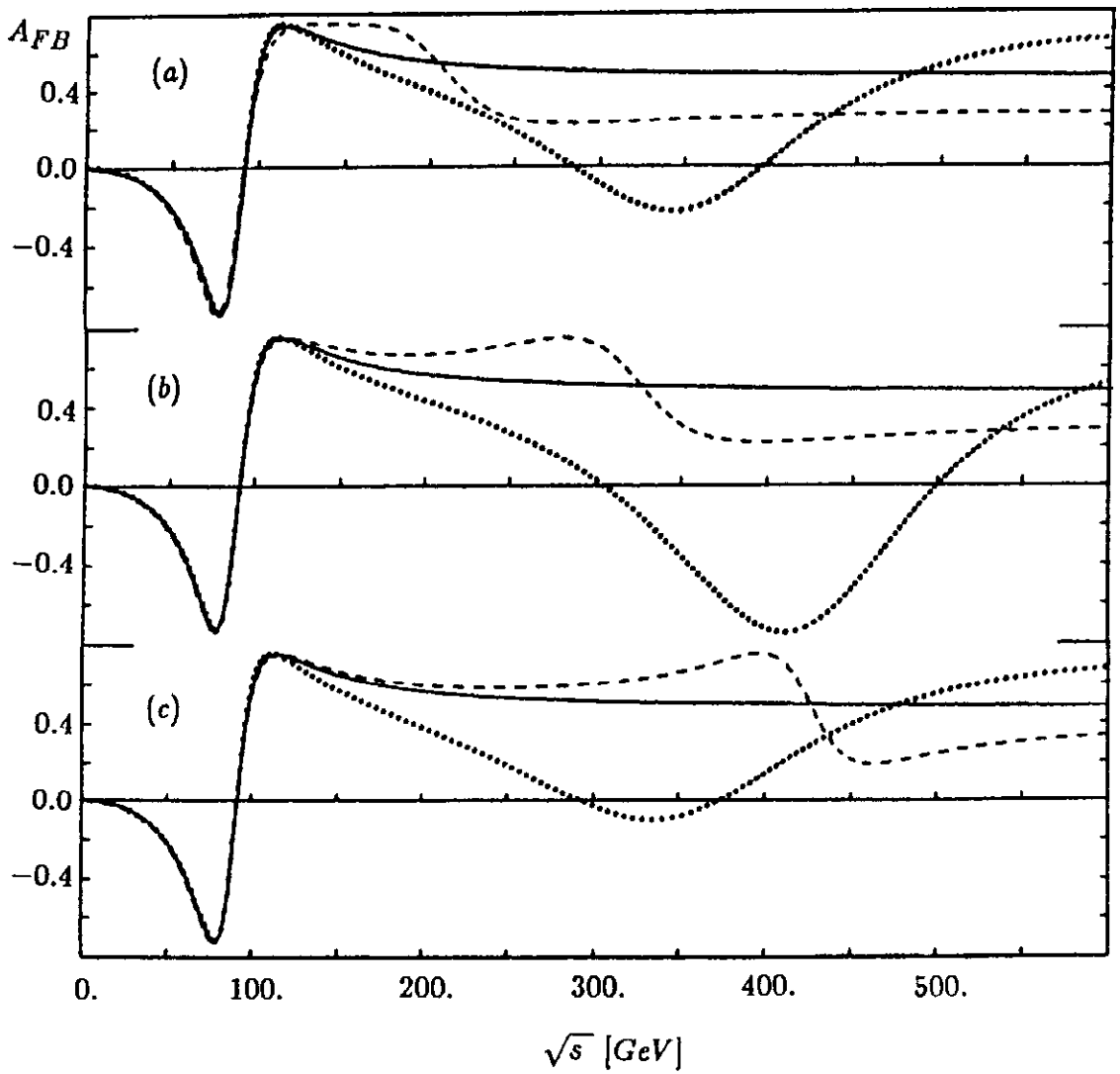

Fig. 4

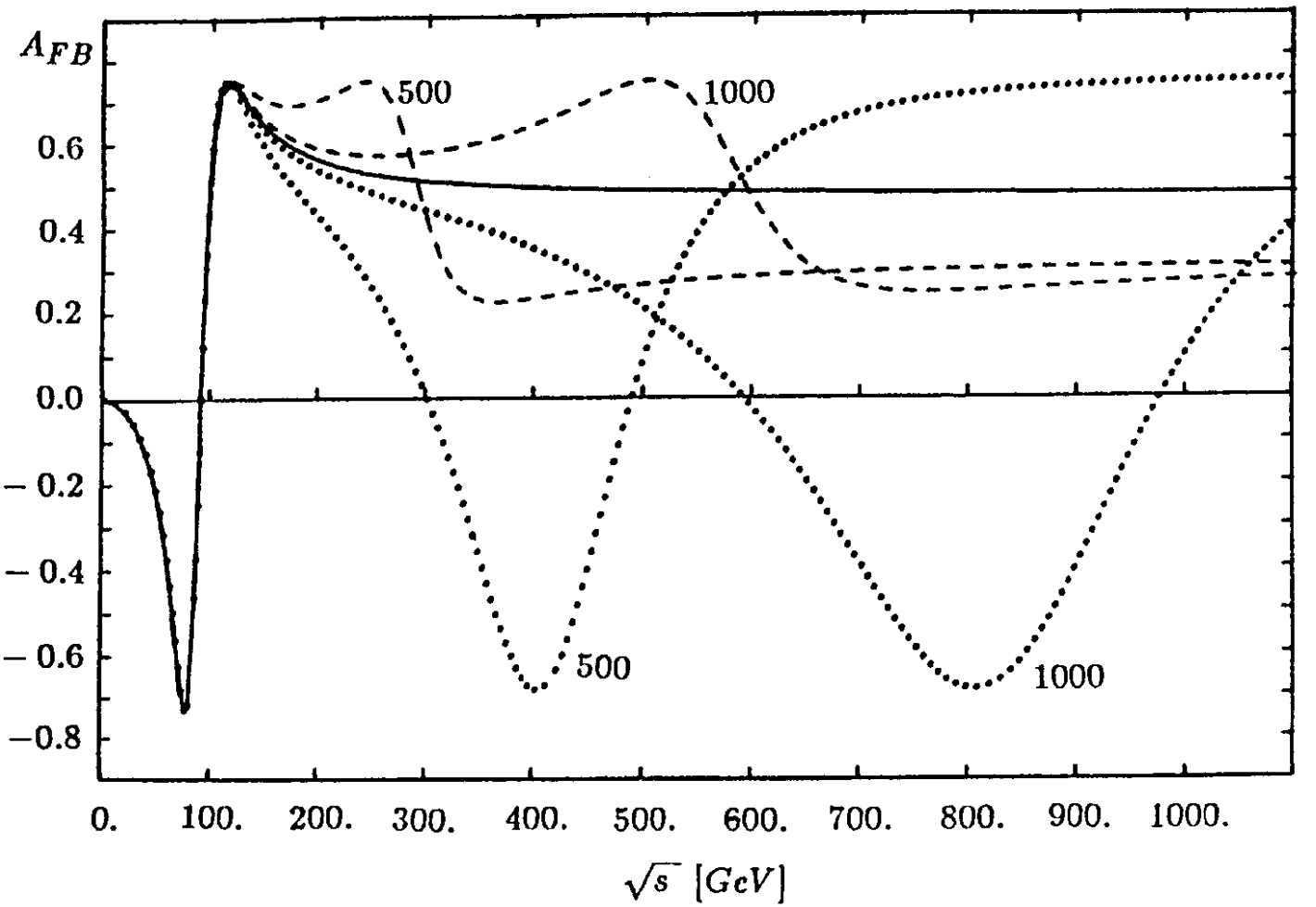
A_{FB}
0.6
0.4
0.2
0.0
− 0.2
− 0.4
− 0.6
−0.8
500
1000
500
1000
0.
100.
200.
300.
400.
500.
600.
700.
800.
900.
1000.
$\sqrt{s}$ [GeV]

Fig. 5

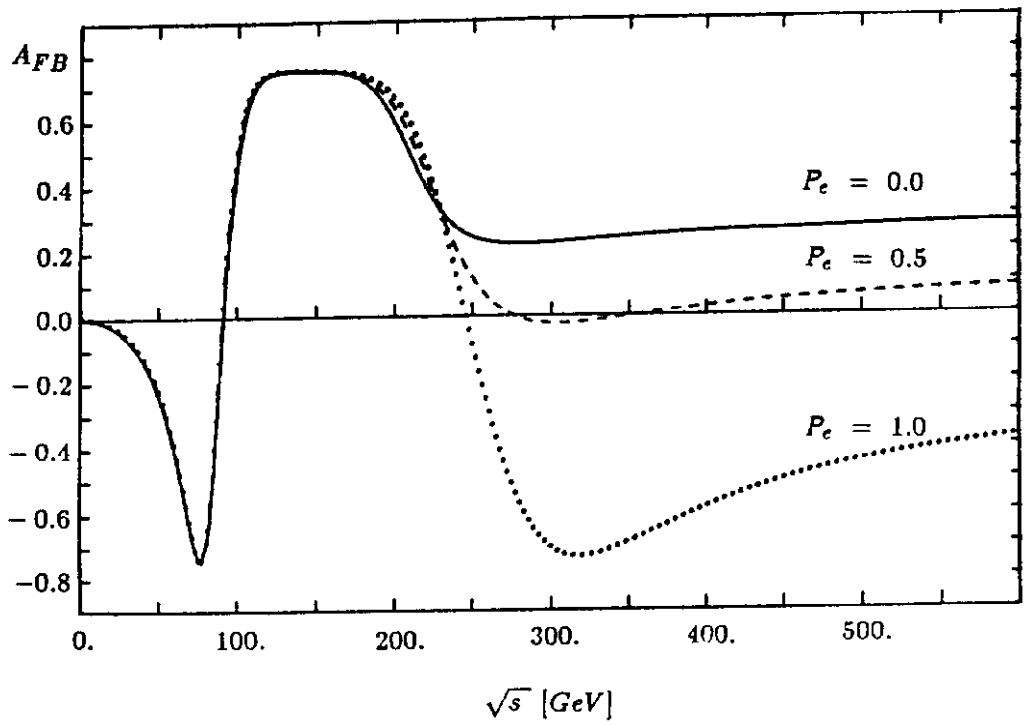
A_{FB}
0.6
0.4
0.2
0.0
− 0.2
− 0.4
− 0.6
−0.8
0.
100.
200.
300.
400.
500.
P_e = 0.0
P_e = 0.5
P_e = 1.0
$\sqrt{s}$ [GeV]

Fig. 6a

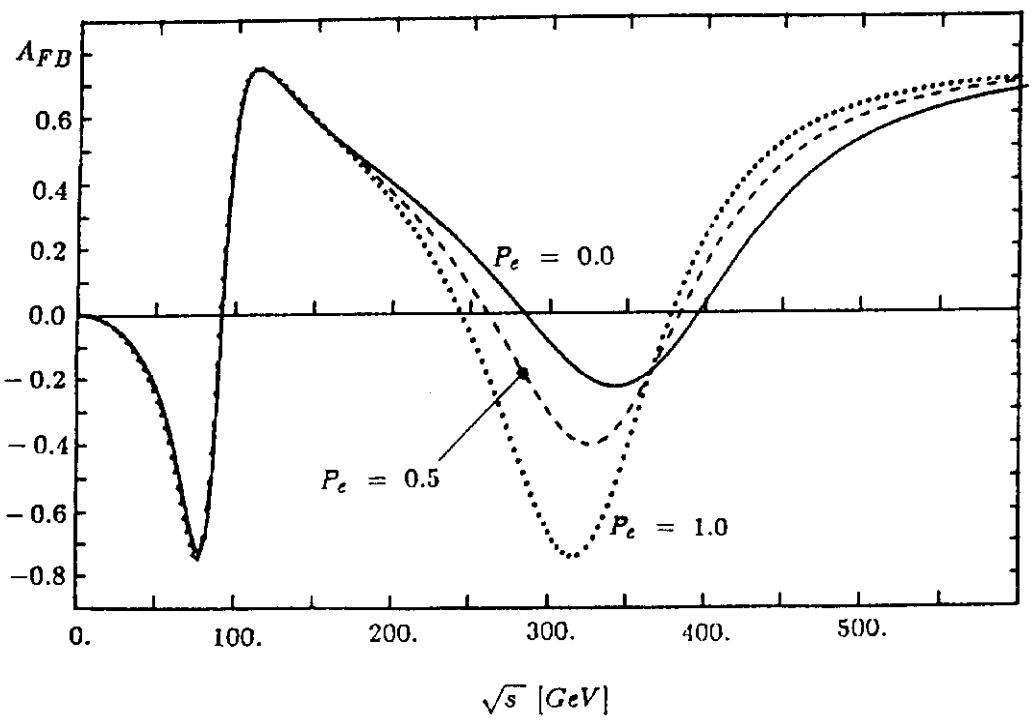
A_{FB}
0.6
0.4
0.2
0.0
− 0.2
− 0.4
− 0.6
−0.8
0.
100.
200.
300.
400.
500.
P_e = 0.0
P_e = 0.5
P_e = 1.0
$\sqrt{s}$ [GeV]

Fig. 6b

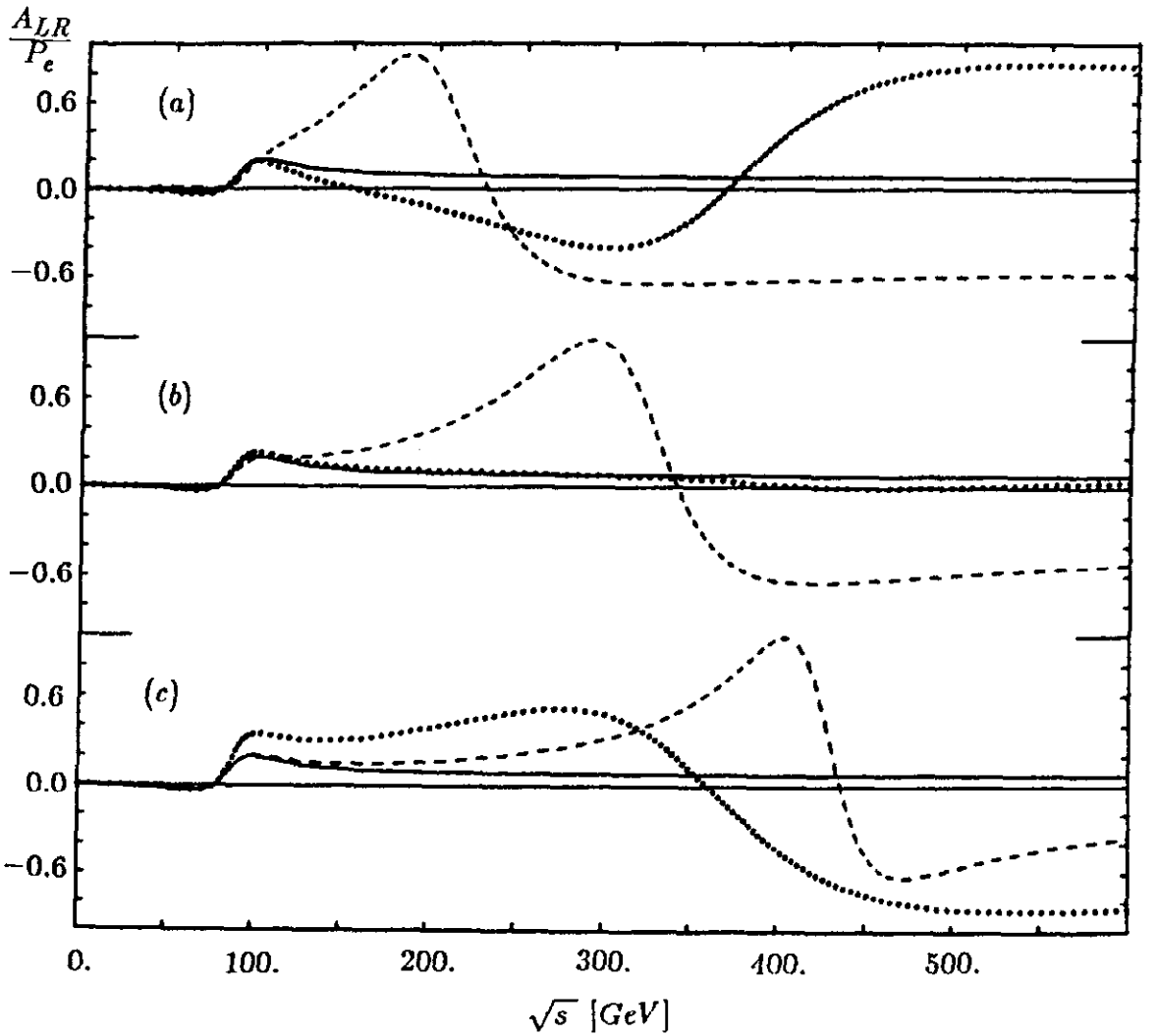
$\frac{A_{LR}}{P_e}$
0.6
0.0
−0.6
(a)
0.6
0.0
−0.6
(b)
0.6
0.0
−0.6
(c)
0.
100.
200.
300.
400.
500.
$\sqrt{s}$ [GeV]

Fig. 7

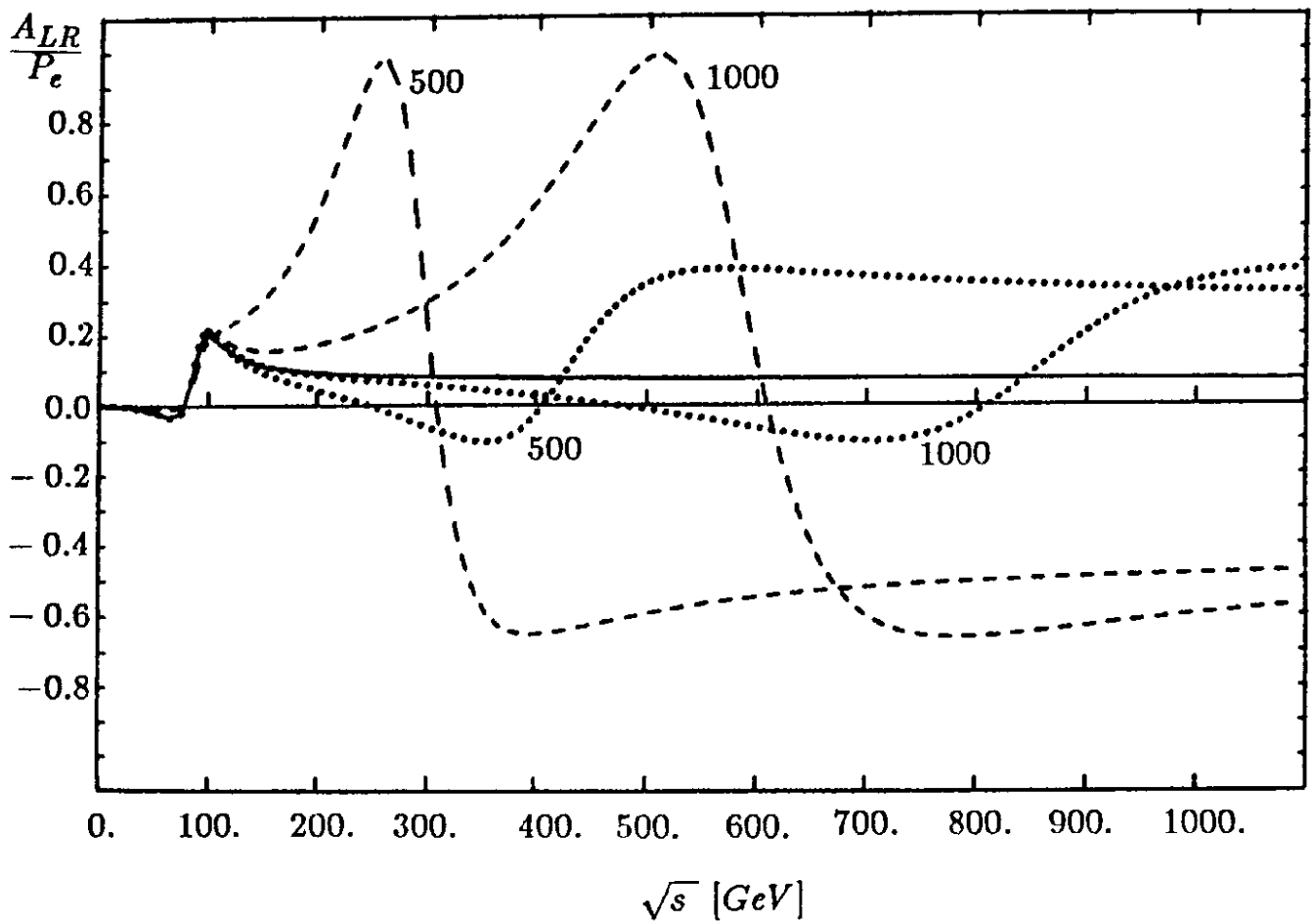
$\frac{A_{LR}}{P_e}$
0.8
0.6
0.4
0.2
0.0
− 0.2
− 0.4
− 0.6
−0.8
500
1000
500
1000
0.
100.
200.
300.
400.
500.
600.
700.
800.
900.
1000.
$\sqrt{s}$ [GeV]

Fig. 8

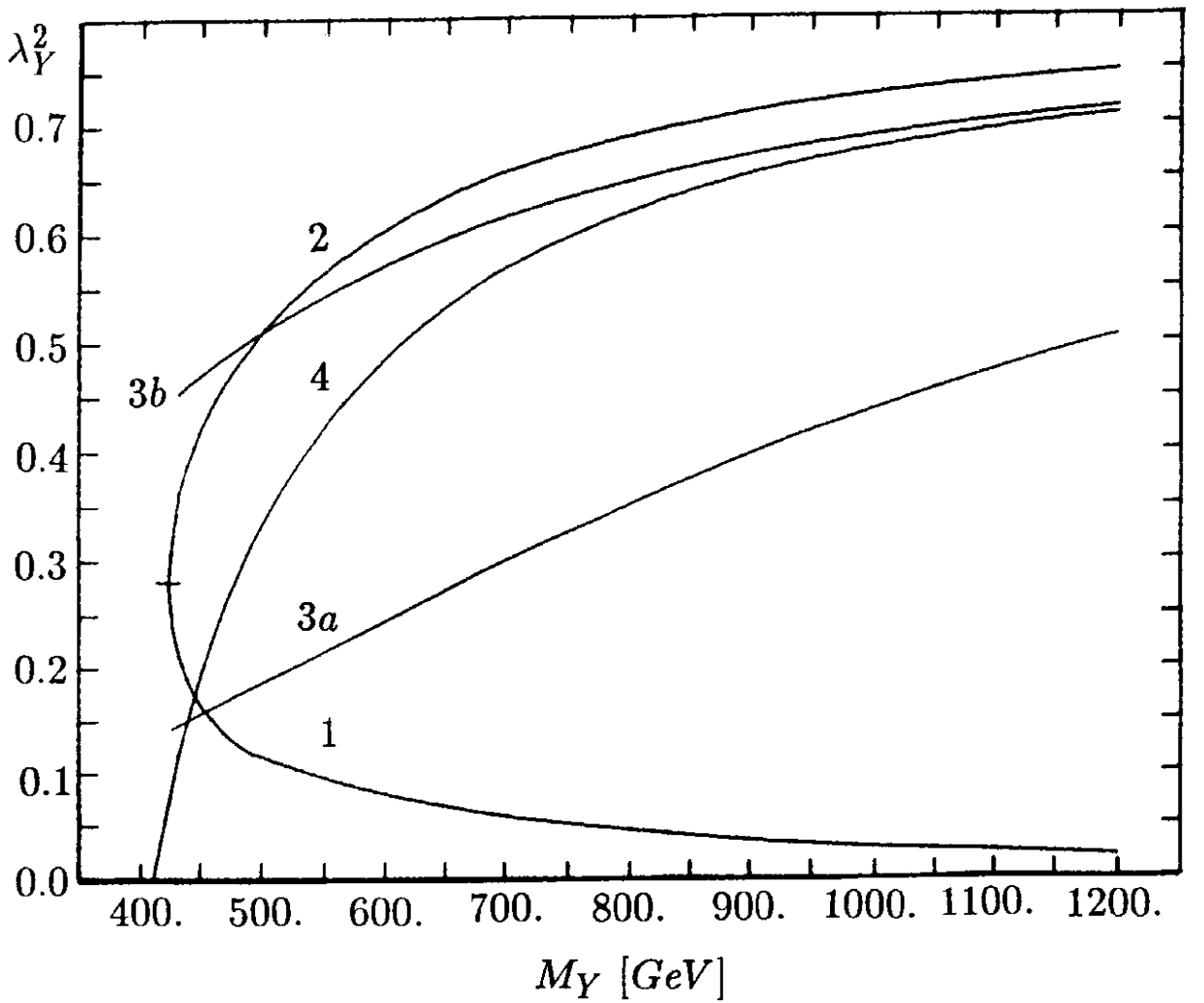
λ_Y^2
0.7
0.6
0.5
0.4
0.3
0.2
0.1
0.0
2
3b
4
3a
1
400.
500.
600.
700.
800.
900.
1000.
1100.
1200.
M_Y [GeV]

Fig. 9

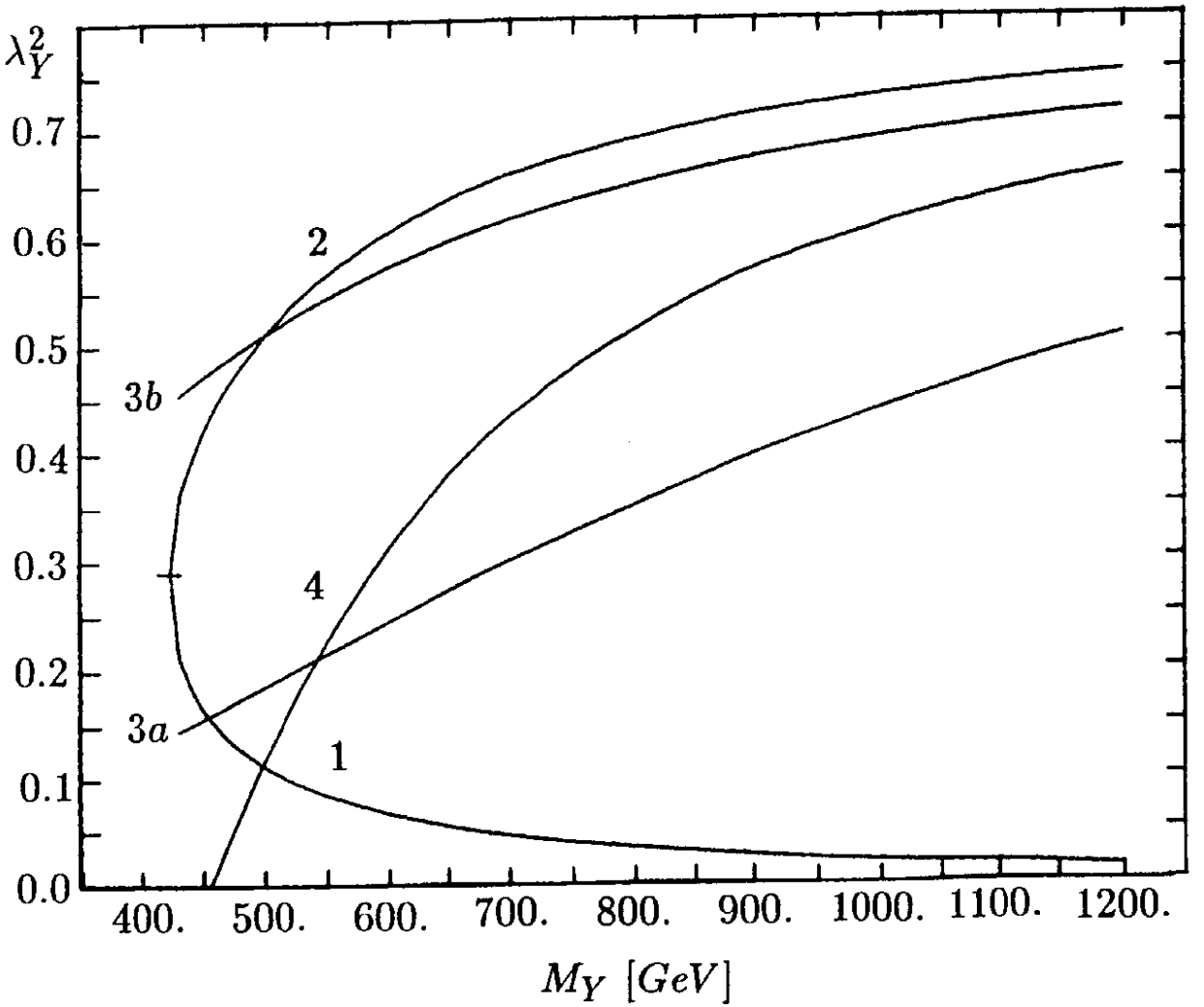
λ_Y^2
0.7
0.6
0.5
0.4
0.3
0.2
0.1
0.0
2
3b
4
3a
1
400.
500.
600.
700.
800.
900.
1000.
1100.
1200.
M_Y [GeV]

Fig. 10

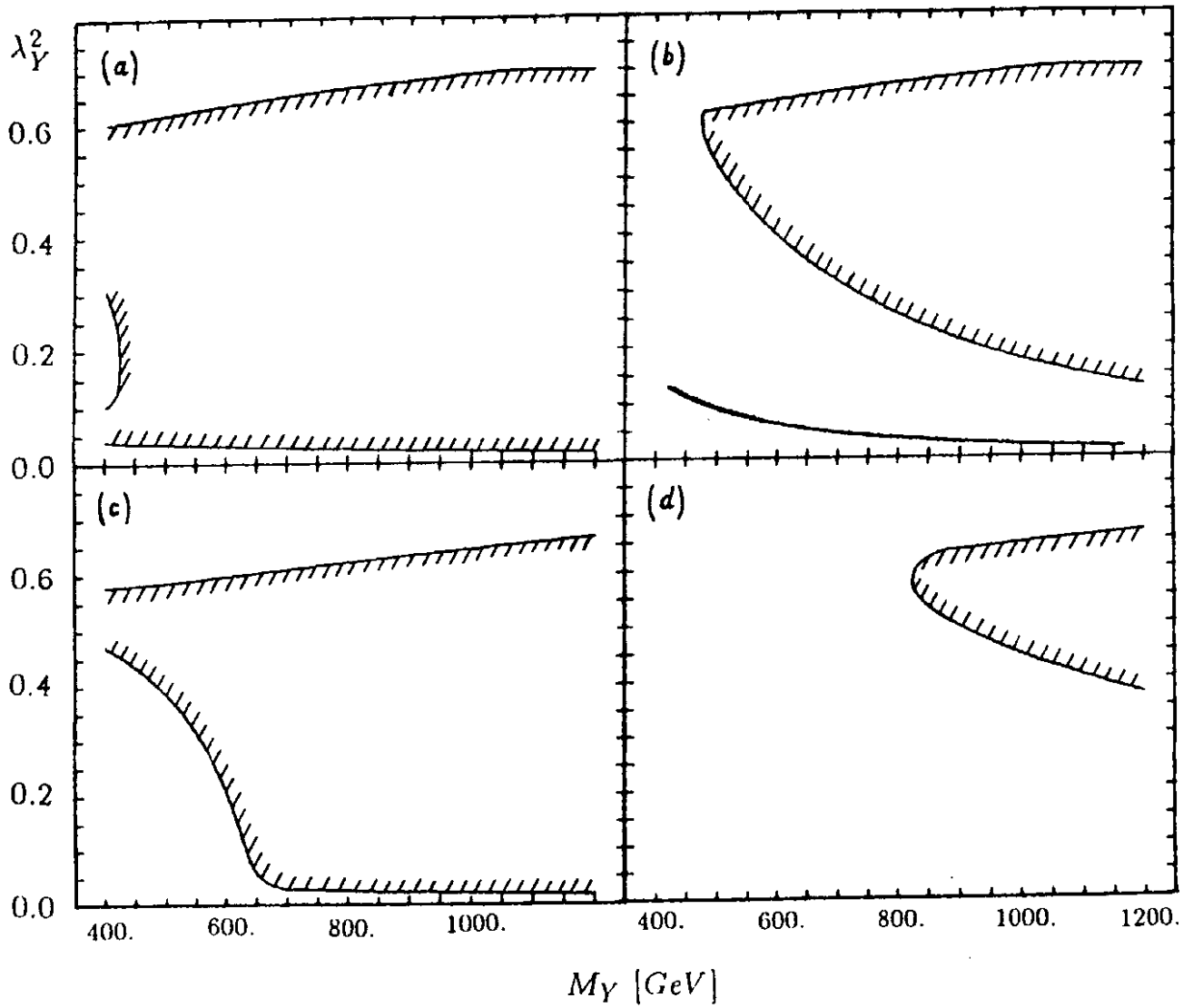

Fig. 11

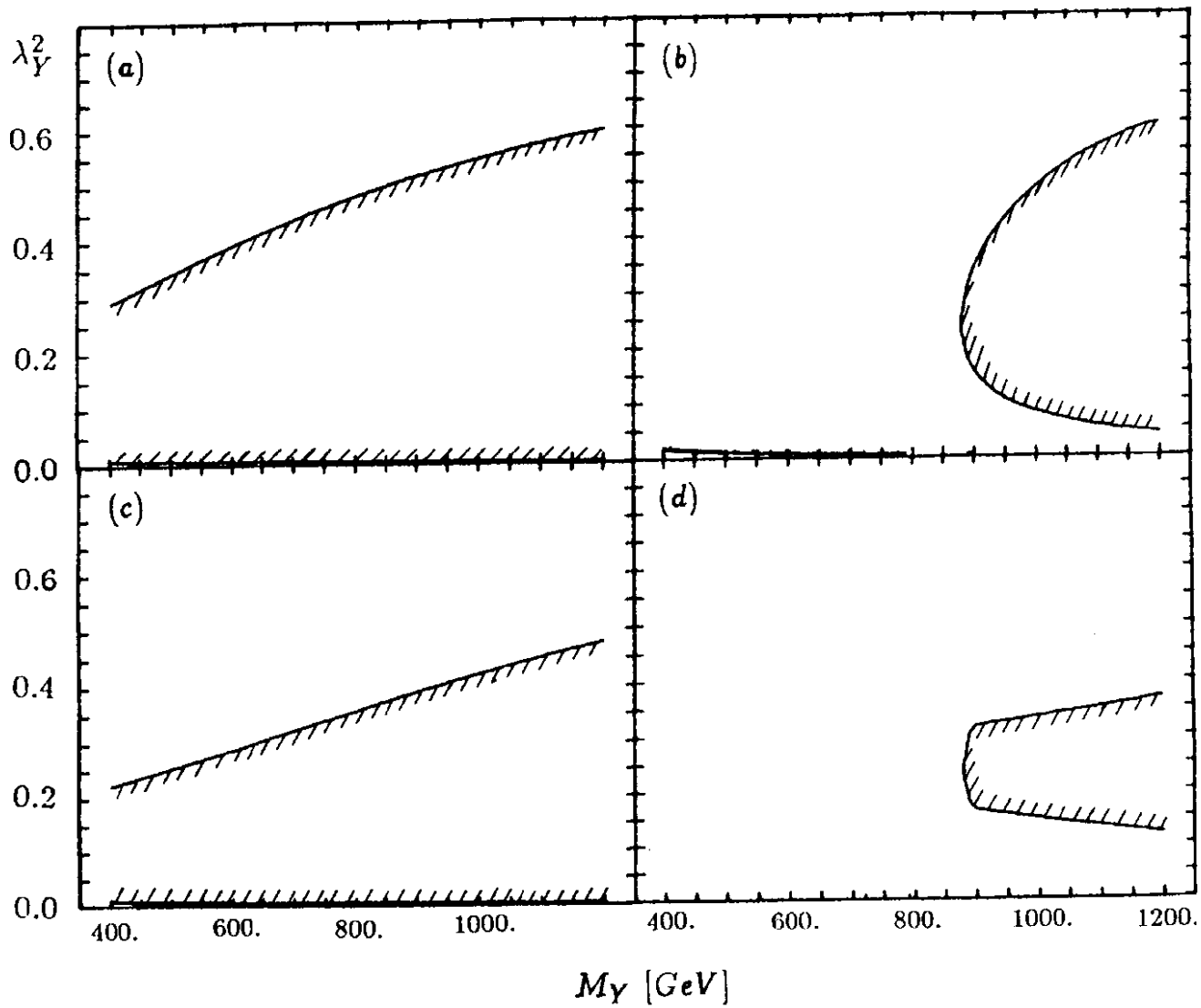

Fig. 12

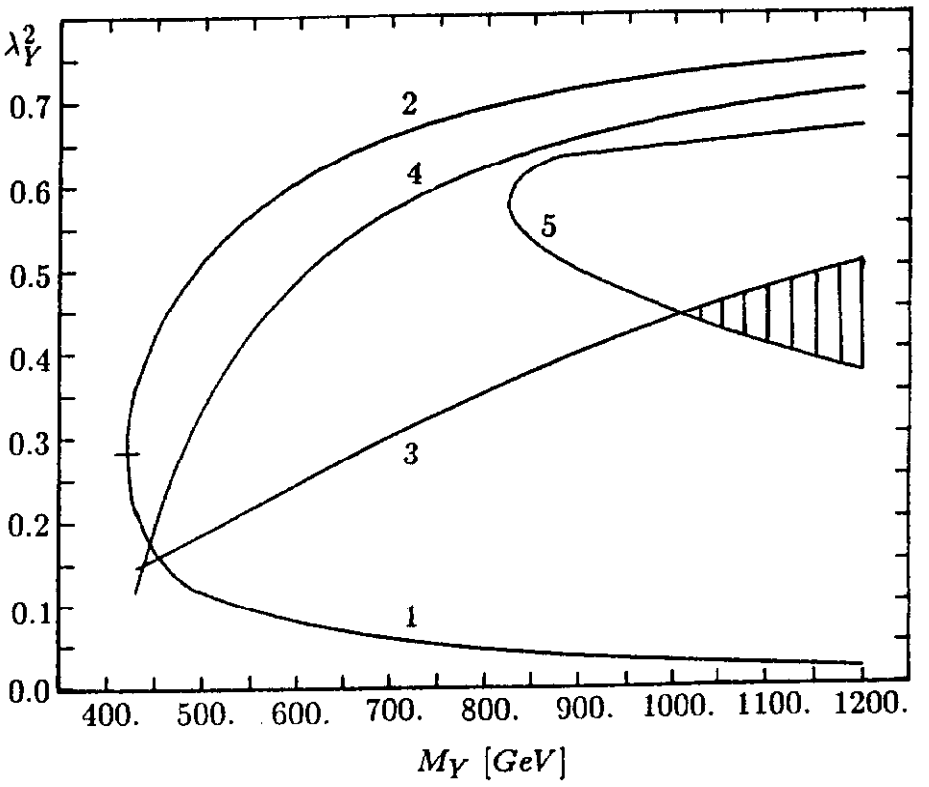

Fig. 13a

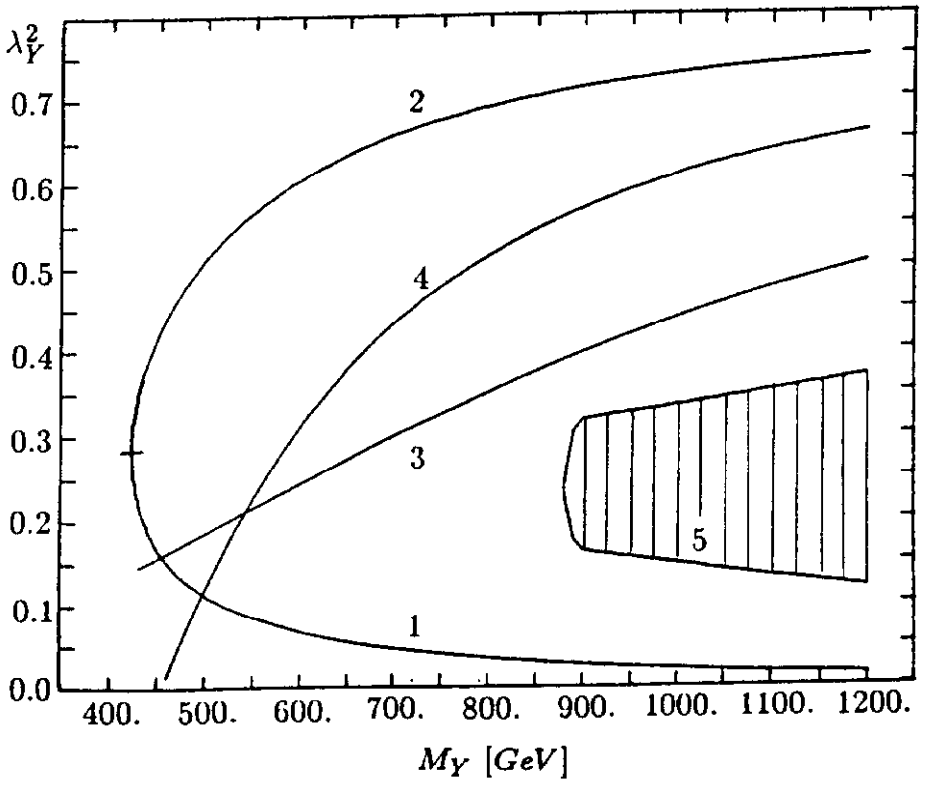

Fig. 13b